NITROUS OXIDE (N_2O) in MACQUARIE HARBOUR, TASMANIA

Maxey, Johnathan Daniel[1,2], Neil D. Hartstein[2], Hermann W. Bange[3], Moritz Müller[1]

[1]Faculty of Engineering, Computing and Science, Swinburne University of Technology, Kuching 93350, Malaysia
[2]ADS Environmental Services, Kota Kinabalu, Sabah, 88400, Malaysia
[3]GEOMAR Helmholtz Centre for Ocean Research Kiel, Wischhofstr. 1-3, 24148 Kiel, Germany

Correspondence to: Johnathan Daniel Maxey, Neil D. Hartstein, Hermann W. Bange, and Moritz Müller

Abstract.

Fjord-like estuaries are hotspots of biogeochemical cycling due to steep physicochemical gradients. The spatiotemporal distribution of nitrous oxide (N_2O) within many of these systems is poorly described, especially in the southern hemisphere. The goal of this study is to describe the spatiotemporal distribution of N_2O within a southern hemisphere fjord-like estuary, describe the main environmental drivers of this distribution, the air/sea flux of N_2O, and the main drivers of N_2O production. Sampling surveys were undertaken in Macquarie Harbour, Tasmania to capture N_2O concentrations and water column physicochemical profiles in winter (July 2022), spring (October 2022), summer (February 2023), and autumn (April 2023). N_2O samples were collected from mid water depths at the ocean (5m) and minor river (1m) endmembers, 2m from the bottom (10m) at the major river endmember, and at 5 depths through the water column at 4 stations within the main harbour body.

Results indicate that N_2O was consistently supersaturated (reaching 170% saturation) below the system's freshwater lens where oxygen concentrations are often hypoxic, but infrequently anoxic. In the surface lens, levels of N_2O saturation vary with estimated river flow and with proximity to the system's main freshwater endmember. The linear relationship between apparent oxygen utilization and ΔN_2O saturation indicates that nitrification is the process generating N_2O in the system. When river flow was high (July and October 2022), surface water N_2O was undersaturated (as low as 70%) throughout most of the harbour.

When river flow was low (February and April 2023) N_2O was observed to be supersaturated at most stations. Calculated air/sea fluxes of N_2O indicated that the system is generally a source of N_2O to the atmosphere under weak river flow conditions and a sink during strong river flow conditions. The diapycnal flux was a minor contributor to surface water N_2O concentrations, and subhalocline N_2O is intercepted by the riverine surface lens and transported out of the system to the ocean during strong river flow conditions. In a changing climate, Western Tasmania is expected to receive higher winter rainfall and lower summer rainfall which may augment the source and sink dynamics of this system by enhancing the summer / autumn efflux of N_2O to the atmosphere.

This study is the first to report observations of N_2O distribution, generation processes, and estimated diapycnal / surface N_2O fluxes from this system.

1. Introduction

Despite the fact that fjords and fjord-like estuaries represent only a small portion of the coastal area worldwide, they are responsible for sequestering 11% of the global organic carbon (C) burial along terrestrial margins (**Smith *et al.*, 2015**; **Bianchi *et al.*, 2018**, **2020**). These systems are significant sources of greenhouse gasses (GHG) to the atmosphere (**Wilson *et al.*, 2020**; **Rosentreter *et al.*, 2023; Bange *et al.*, 2024**). Many are heavily stratified with strong water column physicochemical gradients (**Acuña-González *et al.*, 2006; Inall and Gillibrand, 2010; Hartstein *et al.* 2019; Salamena *et al.*, 2021, 2022; Maxey *et al.* 2022**). These gradients can be influenced by mesoscale climate drivers like North Atlantic Oscillation (NAO) and Southern Annular Mode SAM (see **Austin and Inall 2002; Gillibrand *et al.*, 2005; Maxey *et al.*, 2022**) and local scale drivers like fresh water input and marine intrusions (**Inall and Gillibrand 2010; Hartstein *et al.*, 2019; Maxey *et al.*, 2020; Salamena *et al.*, 2022**).

Nitrous oxide (N_2O) is a potent greenhouse gas (GHG) whose increased presence in the atmosphere is primarily driven by emissions from agricultural soils (**Tian *et al.*, 2020, 2023**). With a global warming potential nearly 300 times that of CO_2, N_2O is a key focus of climate studies (**Myhre *et al.*, 2013**; **Etminan *et al*., 2016; Eyring *et al.*, 2021; Forster *et al.*, 2021**). Biological N_2O production occurs through the microbially mediated processes of ammonia oxidation, nitrite (NO_2^-) reduction, and nitrate (NO_3^-) reduction (**Kuypers *et al.*, 2018**). In marine systems N_2O production is influenced by environmental conditions such as dissolved oxygen (DO) availability, inorganic nitrogen (N) availability, light availability, temperature (*e.g.* **Raes *et al.*, 2016**), pH (*e.g.* **Breider *et al.*, 2019**), and microbial community composition (*e.g.* **Wu *et al.* 2020**). Many coastal systems are experiencing a reduction in DO availability (**Limburg *et al.*, 2020; Testa *et al.*, 2023**) and an increased presence of N_2O as a consequence (**Laffoley and Baxter 2019**; **Ji *et al.*, 2020**; **Wilson *et al.*, 2020**; **Wan *et* al., 2022; Orif *et al.*, 2023; Resplandy *et al.*, 2024**).

Estuarine systems often have disproportionately high biological productivity relative to other marine systems (**Walinsky *et al.*, 2009; Gilbert *et al.*, 2010; Bianchi *et al.*, 2018, 2020**). This also applies to N_2O dynamics with approx. 33% of marine N_2O emissions coming from estuaries (**Bange *et al.*, 1996; Seitzinger *et al.*, 2000**; **Murry *et al.*, 2015**; **Reading, 2022; Rosentreter *et al.*, 2023**). Estuaries can act as net sinks (**Maher *et al.*, 2016; Wells *et al.*, 2018**) or sources (**De Bie *et al.*, 2002; Zhang *et al.*, 2010; Sánchez-Rodríguez *et al.*, 2022**) of N_2O depending on physical drivers of air/sea fluxes including waterbody/atmospheric concentration gradients, current velocities, depth, and wind speed (**Wells *et al.*, 2018**; **Bange *et al.* 2019**). Other factors include land use modification (**Reading *et al.*, 2020; Chen *et al.*, 2022**) and the presence of microplastics (**Chen *et al*, 2022**). Despite the advancements made thus far, our understanding of marine N_2O distribution and atmospheric emissions is poorly constrained and needs improvement (**Bange *et al.*, 2019, 2024**), especially in southern hemisphere fjord-like systems (**Yevenes *et al.*, 2017**). Much of the current uncertainty lies with a lack of in-situ data describing seasonal N_2O dynamics to constrain global emissions models (**Bange *et al.*, 2019**).

The purpose of this study was (1) to investigate the distribution and seasonal variability of N_2O concentrations and emissions in a southern hemisphere fjord-like estuary and (2) to decipher the major physical and biological drivers of these emissions.

2. Methods

2.1 Study Area

Macquarie Harbour is a southern hemisphere fjord-like estuary located on Tasmania, Australia's west coast (**Figure 1**). The harbour is oriented NW by SE, and is approximately 33 km long, 9 km wide, with a surface area of 276 km^2. The mouth of the harbour is constricted by a shallow (4-8m), long (14km) sill known as "Hells Gates". Hells Gates muffles tidal forcing resulting in harbour water levels primarily determined by river flow and wind set up (**Hartstein *et al.,* 2019**). The morphology of this system results in sharp gradients of DO, salinity, and temperature which are seasonally dependant (**Creswell *et al.,* 1989**; **Hartstein *et al.,* 2019**; **Maxey *et al.,* 2022**). In surface waters dissolved oxygen (DO) concentrations are nearly always in equilibrium with the air but decrease sharply through the halocline (~8m to 15m). There is almost no DO produced below the halocline (8m to 12m deep) due to high chromophoric dissolved organic matter (CDOM) levels limiting primary production at the surface (**Maxey *et al.,* 2017, 2020**). Subhalocline layers (~15m to a few meters from the bottom) are observed to have DO concentrations below 62.5 µM more than 50% of the time (*see* **Maxey *et al.,* 2022**). Near the seabed, episodic marine intrusions (deep water renewal) refresh the supply of DO near the mouth of the system but refresh the upper reaches of the harbour less frequently (*see* **Andrewartha and Wild-Allen 2017; Hartstein *et al.,* 2019**; **Maxey *et al.,* 2022**). This process is driven by low atmospheric pressure, sustained NW winds, and low catchment rainfall which itself is influenced by Southern Annular Mode (SAM) (**Hartstein *et al.,* 2019; Maxey *et al.,* 2022**). In the harbour's upper reaches DO concentrations fall below 31 µM nearly a third of the time (**Maxey *et al.,* 2022**). Hydrodynamic and oxygen tracer numerical model simulations of the harbour by **Andrewartha and Wild-Allen (2017)** estimate that 50% of the harbour's basin waters are replaced every 65 days during low river flow conditions and approximately 110 days during normal flow conditions.

The main source of freshwater to the harbour is located on its southeast end (the Gordon River) and drains a nearly pristine catchment (including the Franklin River) of approximately 5,682 km^2 (**Macquarie Harbour Dissolved Oxygen Working Group, 2014**; **Fig 1**). The Gordon River discharges an estimated 180,000 tons organic carbon (OC) per year into the estuary (**Maxey *et al.,* 2020, 2022**). It should be noted that this area receives the some of the highest rainfall (more than 2,500 mm $year^{-1}$) volume in Australia (**Dey *et al.,* 2019**). The King River, located on the harbour's northern end, is the second largest contributor of fresh water to the estuary and drains a catchment area of 802 km^2. Unlike the Gordon River, the King River has a history of receiving treated mining (*e.g.* copper) effluent and transporting this to the harbour (**Carpenter *et al*., 1991; Teasdale *et al*., 2003**).

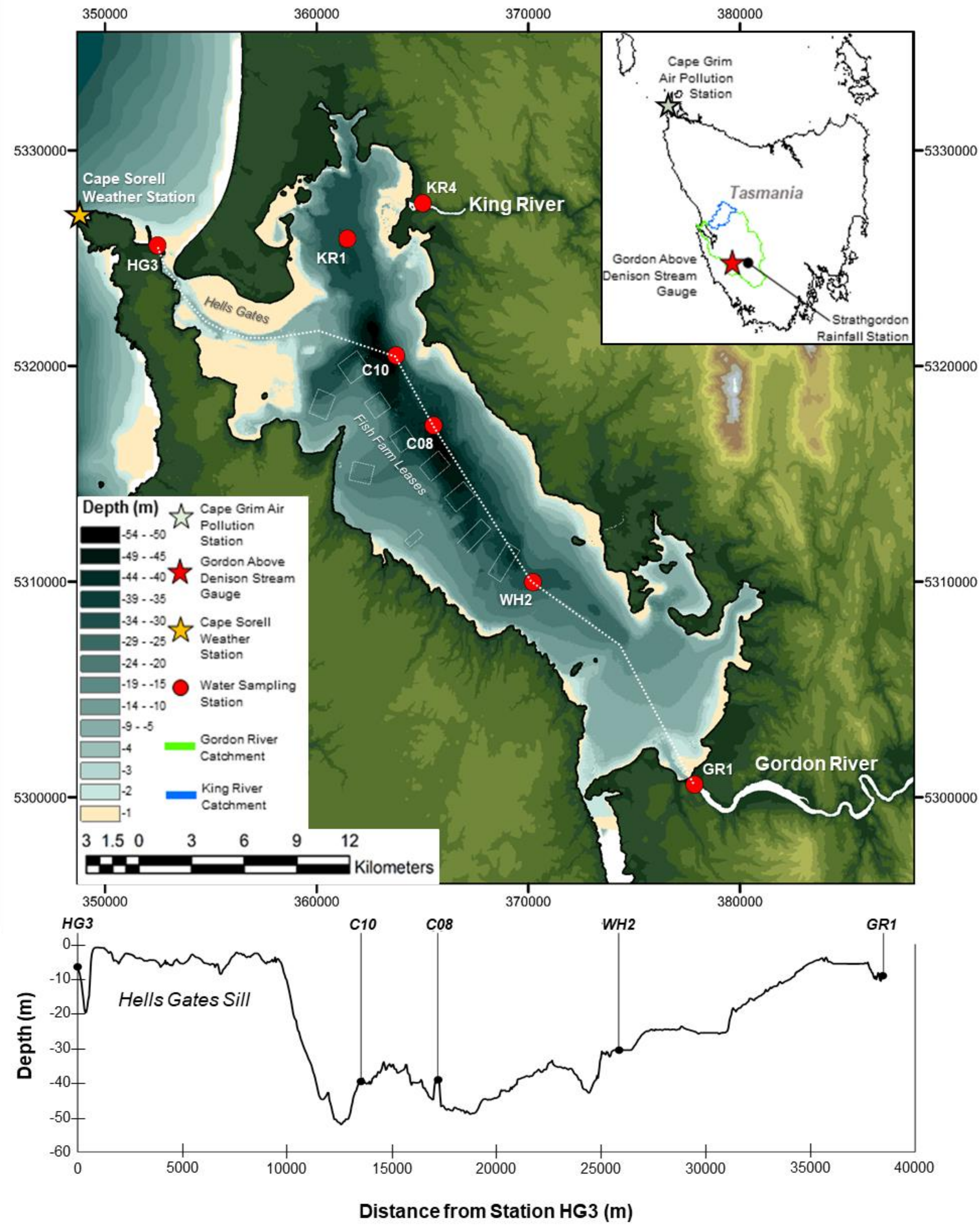

Figure 1: Macquarie Harbour, Tasmania. Water sampling stations shown with red circles; Cape Grim Air Pollution monitoring station shown as a green star (see inset map). Cape Sorell Weather Station shown as an orange star. Gordon Above Denison stream gauge shown as a red star (see inset map). Aquaculture lease boundaries are shown as hollow rectangles. Lease locations are sourced from Land Information Systems Tasmania (LISTmap - https://maps.thelist.tas.gov.au/). Station names reflect general harbour locations where KR1 indicates King River 1; C10 and C08 indicate Central Harbour 10 and 08 respectively; WH2 indicates World Heritage Area 2; and GR1 indicates Gordon River station 1. Coordinates are displayed in GDA_1994_MGA_Zone_55. Bathymetry through the system shown as a dashed line, note that this track excludes stations KR4 and KR1.

2.2 Experimental Design

Nitrous oxide distribution was assessed by collecting water samples across 7 stations, including the harbour's endmembers (mouths of the Gordon and King Rivers as well as the harbour mouth at Hells Gates Inlet; *see* **Figure 1** and **Table 1**) and stations along the longitudinal axis of the harbour where the deepest basins are located (named KR1, C10, C08, and WH2). Samples collected at endmember stations were collected from a single depth as these stations are shallow. Samples in the harbour body were collected at 5 depths from the surface (2m) to approx. 1m from the seabed. Collection campaigns were conducted in July 2022, October 2022, February 2023, and April 2023. At each station and depth, three replicate vials (n = 3) were collected for the determination of N_2O concentration.

2.3 Field Sampling

At each station, water quality sonde profiles were collected from the surface to the seabed at 1 meter intervals using a YSI EXO-1 equipped with optical DO (accuracy from 0 to 625 µM ± 3 µM or 1% of reading whichever is greater; precision is 0.03 µM), salinity (accuracy ± 0.1 or 1% of reading whichever is greater; precision is 0.01), temperature (accuracy is ± 0.15 ºC; precision is 0.01 ºC), and depth sensors. Sonde calibration was checked and corrected (when needed) each sampling period.

Water samples were collected at various depths (see **Table 1**) using a 5 L Niskin bottle sampler. Water sample parameters include dissolved Total Ammoniacal N (NH_3 + NH_4^+) (TAN), NO_3^-, and N_2O. N_2O samples were collected in triplicate immediately after retrieval of the Niskin bottle by transferring water from the bottle through silicone tubing into a 20 mL borosilicate vial. Sample water was added to the vial by placing the tubing at the bottom and allowing the vial to overflow several volumes before sealing with a butyl rubber stopper and aluminium crimp. After ensuring the sample vial was bubble free, 50 µL of saturated mercury chloride ($HgCl_2$) solution was injected into the sample to arrest biological activity. All N_2O samples were shipped to GEOMAR in Kiel, Germany for analysis. Samples were measured in July/August 2023 within 4 to 12 months after sampling and were not affected by the storage time (**Wilson *et al.*, 2018**).

Water collected for dissolved inorganic N was filtered immediately using 0.45 µm polyethersulfone syringe filters (Whatman Puradisc). Samples were stored in a chilled dark container until being transported to Analytical Services Tasmania in Hobart, Australia for analysis. Dissolved Total TAN and NO_3^- were analysed using a Lachat Flow Injection Analyser. TAN and NO_3^- analyses used methods based on APHA Standard methods (2005) 4500-NH_3 H (reporting limit 0.005 mg L^{-1}) and 4500 - NO_3^- L^{-1} (reporting limit 0.002 mg L^{-1}).

Table 1: Sampling stations showing coordinates, parameters, and sampling depth (in meters).

Station	Station Depth (m) (MSL)	Dissolved Oxygen Salinity Temperature	N_2O	TAN (NH_3 + NH_4^+)	NO_3^-
HG3 *352484, 5325594*	8	*Every Meter*	*5m*	*5m*	*5m*
KR4 *365018, 5327550*	3	*1m*	*1m*	*1m*	*1m*
KR1 *361316, 5325972*	*36*	*Every Meter*	*2, 12, 20, 30, 35m*	*2, 12, 20, 30, 35m*	*2, 12, 20, 30, 35m*

C10 *363708, 5320464*	*44*	*Every Meter*	*2, 12, 20, 30, 42m*	*2, 12, 20, 30, 42m*	*2, 12, 20, 30, 42m*
C08 *365489, 5317238*	*47*	*Every Meter*	*2, 15, 25, 35, 45m*	*2, 15, 25, 35, 45m*	*2, 15, 25, 35, 45m*
WH2 *370218, 5309894*	*32*	*Every Meter*	*2, 12, 20, 25, 30m*	*2, 12, 20, 25, 30m*	*2, 12, 20, 25, 30m*
GR1 *377784, 5300603*	*12*	*Every Meter*	*10m*	*10m*	*10m*

2.4 Analysis of Rainfall and River Loading Estimation

Rainfall and river discharge were analysed using methods presented in **Maxey *et al.* (2022)** where rainfall and stream gauge data were collected from the Gordon River catchment, Strathgordon rainfall gauge station and the Gordon Above Denison (GAD) stream gauge (**Figure 1**). The rainfall and flow metrics computed include the average daily rainfall over a 20-day period prior to sampling; total accumulated rainfall 20,10, 5, and 3 days prior to sampling; estimated Gordon River flow into the estuary; and measured flow at the GAD stream gauge.

Gordon River flow was estimated by scaling daily rainfall to the size of the catchment and assuming a rainfall and runoff coefficient of 0.70 adopted from a neighbouring catchment with similar land cover, geology, and slope (**Willis, 2008**). Additional streamflow from Gordon River dam releases was estimated by subtracting scaled rainfall contributions to river flow measured at the GAD stream gauge. This flow was added to the estimated runoff entering the harbour. Rainfall and flow data were provided by the Australian Bureau of Meteorology (BOM). NO_3^- and TAN loading was estimated my multiplying the measured concentration of each parameter at station GR1 (*see* **Figure 1** and **Table 1**) by the estimated Gordon River flow.

2.5 Analysis of Water Column N_2O Concentrations, Air/Sea Flux, and Diapycnal Flux

2.5.1 Determination of N_2O Concentrations

Water samples were analysed for N_2O using the static-headspace equilibration method followed by gas chromatographic separation (HP Agilent 5890) and detection with an electron capture detector (ECD) as described in **Bange *et al,* (2019)**, **Bastian (2017)**, and **Kallert (2017)**. The concentration of N_2O in the samples was calculated with the following equation (**Equation 1;** *see* **Bange *et al.*, 2006**):

Equation 1

$$\mathbf{C_{obs}} = \frac{\mathbf{x' P V_{hs}}}{\mathbf{RTPV_{wp}}} + \mathbf{X'\beta P}$$

$\mathbf{C_{obs}}$ is the concentration (nmol L^{-1}) of N_2O in the water sample; **x'** is the measured dry mole fraction of N_2O in the sample vial's headspace; P is the ambient pressure set to 1 atm; $\mathbf{V_{hs}}$ and $\mathbf{V_{wp}}$ are the volumes of the headspace in the vial and water in the vial; **R** is the gas constant; **T** is the temperature during equilibrium; and **β** is the solubility of N_2O (**Weiss and Price, 1980**). The mean relative error of the concentration values obtained was 2.4% (± 0.16).

2.5.2 Estimation of N_2O Air/Sea Fluxes and N_2O Saturations

N_2O air/sea fluxes (**F** in µmol m^{-2} d^{-1}) were estimated using equations from **Zhang *et al.*, (2010)** and **Bange *et al.*,** (**2019**) (**Equation 2)** *Where*:

Equation 2

$$\mathbf{F} = \mathbf{K} * (\mathbf{C_{obs}} - \mathbf{C_{eq}})$$

$\mathbf{C_{obs}}$ is the measured concentration (nmol L^{-1}) of N_2O in the water sample; $\mathbf{C_{eq}}$ is the air-equilibrated seawater N_2O concentration, calculated for in situ temperature and salinity using the solubility data of **Weiss and Price (1980)**. **K** is the gas transfer velocity, which in the absence of direct measurements can be expressed as a function of the wind speed and the Schmidt Number (*Sc*). For this study we sourced daily average wind speed from the Cape Sorrel Weather Station at the northern end of Macquarie Harbour (http://www.bom.gov.au/climate/data/index.shtml station ID 097000; see **Figure 1** for station location). **K** was estimated using relationships in **Nightingale (2000), Raymond and Cole** (**2001**), and **Wanninkhof (2014)**. Fluxes at Macquarie Harbour's endmember stations used **K** values that account for additional forcings like bottom sheer (*see* **Raymond and Cole 2001**; **Zappa e*t al.*, 2003**; **Abril and Borges 2004, Beaulieu *et al.*, 2012; Rosentreter *et al.*, 2021**). Deeper stations in the harbour's main body (*i.e.* KR1, C10, C08, WH2) have surface layers which are separated from the seabed by more than 10 meters. Wind-based K_{600} estimators were used to estimate air-sea flux in those locations (*see* **Nightingale 2000; Raymond and Cole 2001; Wanninkhof 2014**). Atmospheric N_2O for this estimation was sourced from monthly mean baseline greenhouse gas mole fractions measured at the Kennaook / Cape Grim Baseline Air Pollution Station, located in north west Tasmania. This station measures atmospheric N_2O using a gas chromatograph (GC) equipped with an ECD (https://www.csiro.au/en/research/natural-environment/atmosphere/latest-greenhouse-gas-data). N_2O saturation (in %) were computed as N_2O saturation = 100 * (C_{obs} / C_{eq}).

2.5.3 Estimation of Diapycnal N_2O Flux

N_2O diapycnal fluxes ($\mathbf{F_{dia}}$ **; Equation 3**) from basin waters (sample depths of 20m or 25m) to the harbour's surface lens (sample depths of 2m) were estimated as:

Equation 3

$$\mathbf{F_{dia}} = \mathbf{K\rho} \frac{\mathbf{d[N_2O]}}{\mathbf{dz}}$$

Where **z** is depth. Diapycnal diffusivity ($\mathbf{K_\rho}$**; Equation 4**) was computed with the local buoyancy frequency ($\mathbf{N^2}$), **Γ** set to 0.2 (**Osborn 1980**), and **ε** the dissipation rate of turbulent kinetic energy assumed to be on the upper end of values for the mixing zone of stratified systems 1 x 10^{-5} (**Arneborg *et al.*, 2004; Mickett *et al.*, 2004; Fer *et al.*, 2006**).

Equation 4

$$\mathbf{K_\rho} = \mathbf{\Gamma} \frac{\boldsymbol{\varepsilon}}{\mathbf{N^2}}$$

2.6 Data Analysis

The relationships between N_2O saturation and water quality parameters such as DO concentration, salinity, temperature, nitrate, and ammonium concentrations determined using Pearson correlation. Differences in mean N_2O saturation between season, depth and each sampling station were tested using a 2-way ANOVA. Differences between rainfall / river flow metrics between seasons were tested using 1-way ANOVA and where significant differences between seasons were detected pair-wise testing using Bonferroni's correction was undertaken. The relationship between rainfall / river flow metrics, from the Gordon River, and surface water N_2O saturation / N_2O air/sea flux, at each station, was analysed using Pearson correlation. Standard deviation (std. dev.) of the mean air/sea flux and diapycnal flux was computed from error propagated from replicate observations of N_2O wind speed, N_2O concentration, and density (where appropriate) using methods from **Ku (1966).** Contour plots were made with Plotly Chart Studio: Plotly Technologies Inc. Title: Collaborative data science Publisher: Plotly Technologies Inc. Place of publication: Montréal, QC Date of publication: 2015 URL: https://plot.ly

3. Results

3.1 Rainfall and River Loading

Twenty-day rainfall accumulation ranged from a low of 117 mm in July 2022 to a high of 139 mm in April 2023 (*see* **Figure 2a**). Average (± se) daily rainfall was similar across all months and ranged from 5.12 (± 2.57) mm in July 2022 to 5.79 (± 3.03) mm in October 2022 (*see* **Figure 2b**) with no seasonal differences detected (p = 0.4326).

Estimated flow at the Gordon River mouth and GAD stream gauge was greater in July and October 2022 than February and April 2023 (**Figure 2c**). Significant seasonal differences in flow measured at the GAD stream gauge were detected ($p = 5.5 \times 10^{-7}$); with greatest flow in July and October 2022 and decreasing over February and April 2023. July flows at the GAD stream gauge were observed to be 107.6 (± 15.9) $m^3 s^{-1}$ and in April 2023 were observed to be 30.5 (± 2.2) $m^3 s^{-1}$ (**Figure 2d**).

Estimated NO_3^- and TAN loading varied with NO_3^- loads of 1.69 tonnes day^{-1} observed in July 2022, which then dipped to 0.31 tonnes day^{-1} in October 2022 and then increased again to 1.77 and 2.77 tonnes day^{-1} in February and April 2023 (**Figure 2e**). TAN loading mirrored this pattern with peaks occurring in October 2022 and February 2023 and lows occurring in July 2022 and April 2023. N_2O loading from the Gordon River was observed to be 0.015 tonnes day^{-1} in July 2022, 0.012 tonnes day^{-1} in October 2022, 0.015 tonnes day^{-1} in February 2023, and 0.016 tonnes day^{-1} in April 2023 (**Figure 2f**).

3.2 Water Column Physicochemical Profiles

DO profiles at the stations located within the main body of the harbour show a well oxygenated surface layer that rapidly attenuates with depth (**Figure 3A**) through the halocline (**Figure 3B**). There is a prominent riverine surface lens in the main harbour extending to depths of up to 8m depending on sampling period and location within the estuary. Salinity in the surface waters was lower in July and October 2022 (6 to 13) than February and April 2023 (greater than 20). Below the halocline salinity ranged from approx. 28 to 32.

The DO gradient between the surface and subhalocline waters was steeper in October relative to July 2022 with October 2022 DO concentrations approaching single digits (3.1 µM) at station WH2, nearest the Gordon River mouth (*see* **Figure 1**). In general, the subhalocline concentrations of DO were lower with proximity to the Gordon River mouth. The temperature of the freshwater surface layer ranged from about 9 ºC to 19 ºC, but showed little variation below the halocline where temperature ranged between 13 °C to 16 ºC (**Figure 3C**).

Nitrate concentrations in the surface water lens tended to be lower than those observed at subhalocline depths (**Figure 4a**). The greatest NO_3^- concentrations were observed 2m above the seabed at station WH2 in July and October 2022 as well as mid basin depths at stations C10 and C08 during those same periods with concentrations reaching 1.77 µmol. TAN concentrations were often observed below detection limits (0.3 µmol), but were greatest in the surface lens or within the halocline itself when detectable (**Figure 4b**). TAN concentrations at WH2 tended to be found at higher levels through the water column relative to other stations (down to about 20m) reaching 1.53 µmol at 15m in October.

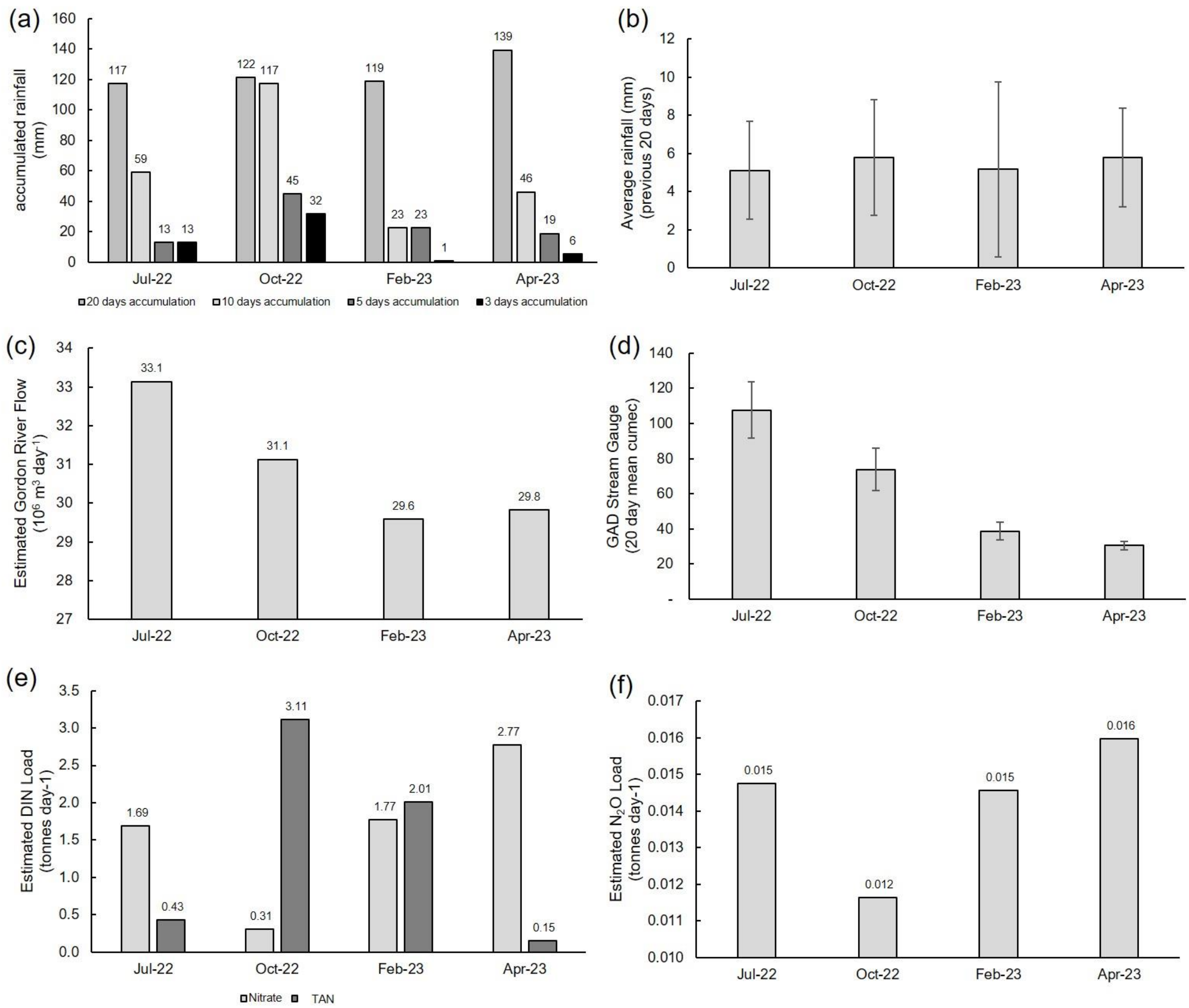

Figure 2: Rainfall and estimated Gordon River loading estimates for each sampling event. A) accumulated rainfall (mm) 10, 5, and 3 days prior to each sampling event; B) average (mean) daily rainfall over a 20 day period prior to each sampling event; C) estimated Gordon River Flow into the harbour in millions of m^3 day^{-1}; D) daily mean flow (m^3 sec^{-1}) over previous 20 days prior to sampling (± standard error) at the Gordon Above Denison Stream Gauge; E) estimated nitrate and ammonium loads entering the harbour from the Gordon River; F) estimated N_2O load (tonnes day^{-1}) entering the harbour from the Gordon River.

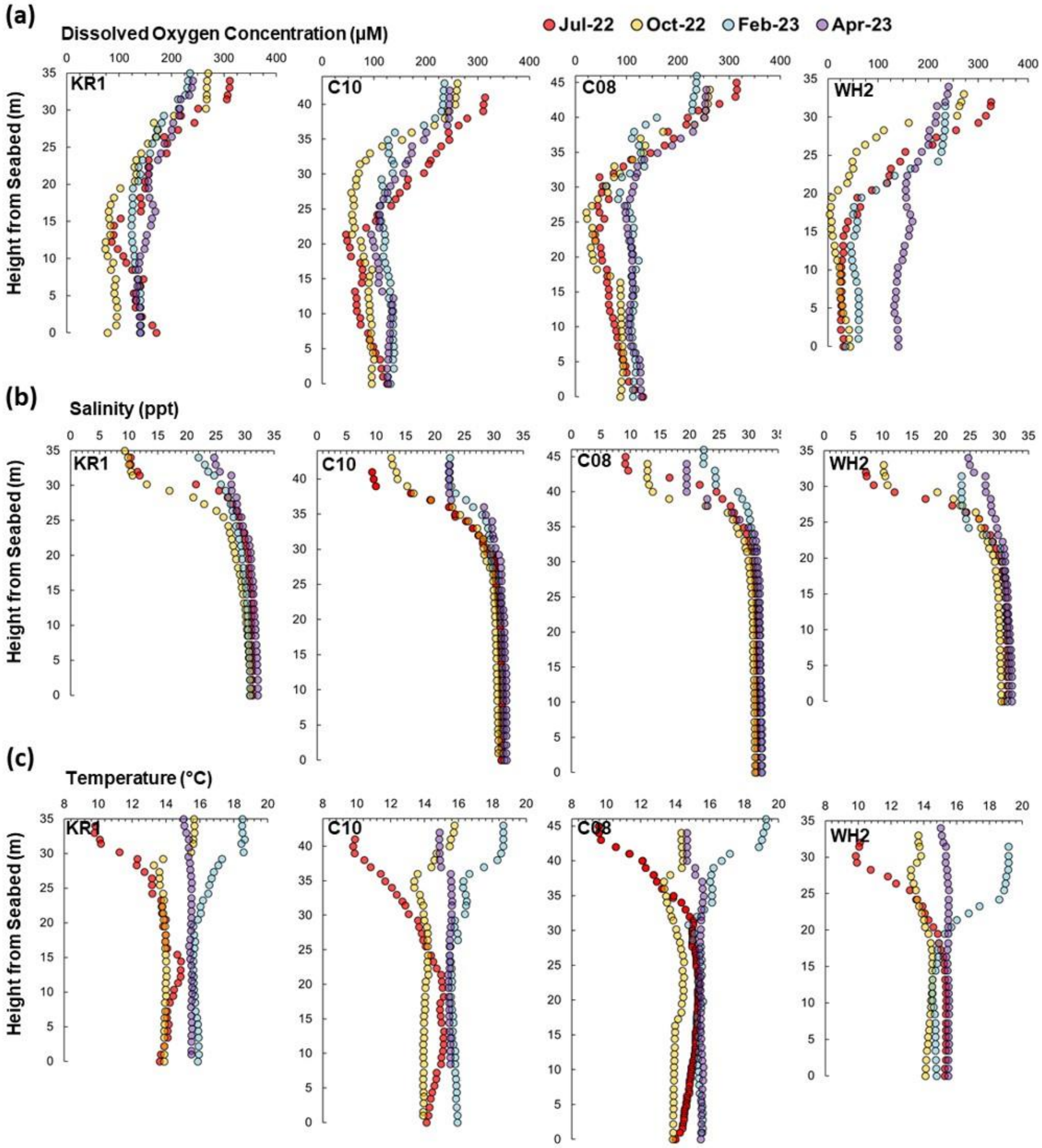

270 **Figure 3: Dissolved oxygen (µM) (Row A), salinity (Row B), and temperature (°C) (Row C) profiles (referencing height from seabed) collected at stations KR1, C10, C08, and WH2 in July 2022 (red dots), October 2022 (yellow dots), February 2023 (blue dots), and April 2023 (purple dots). Measurements were made every 1 meter.**

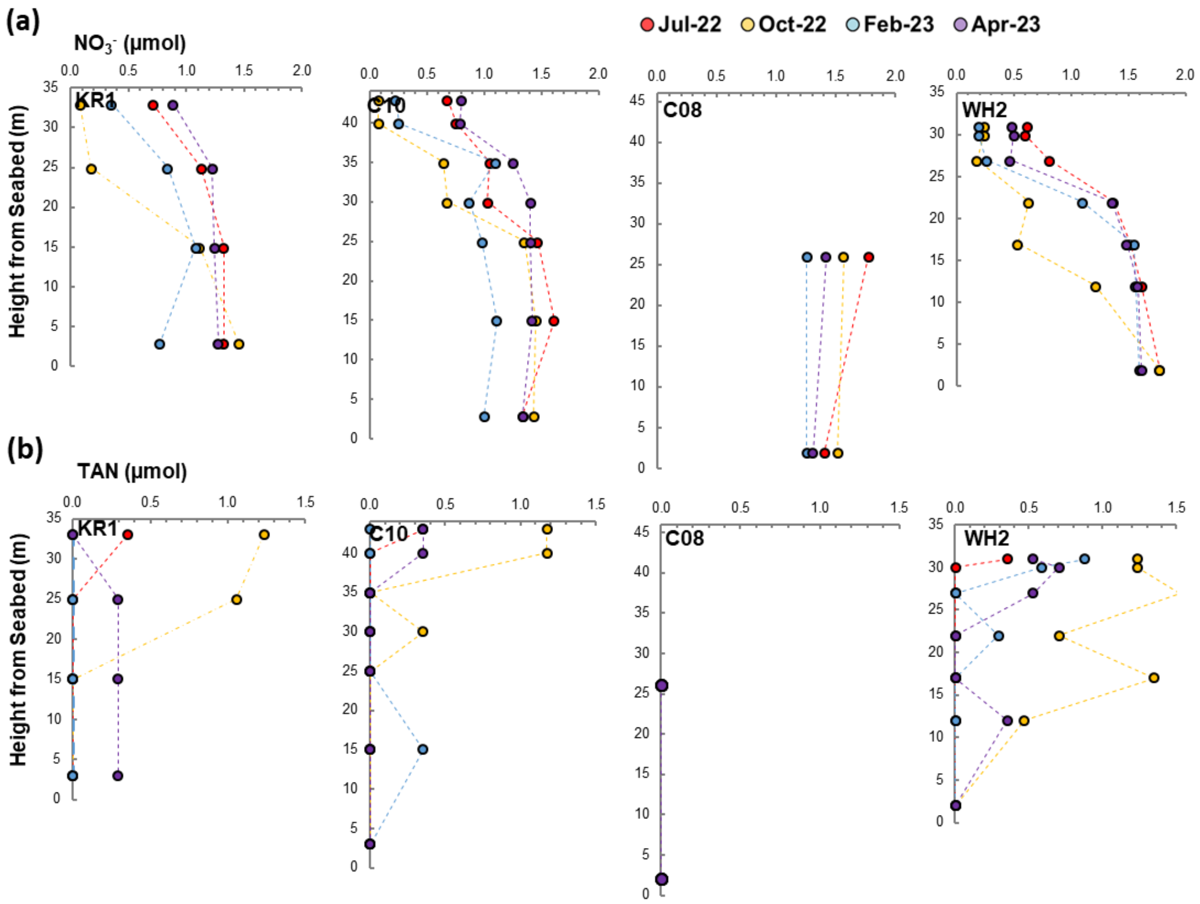

Figure 4: Nitrate NO_3^- (row a) and TAN (row b) concentrations with depth (referencing height from seabed) collected at stations KR1, C10, C08, and WH2 in July 2022 (red dots), October 2022 (yellow dots), February 2023 (blue dots), and April 2023 (purple dots). Data presented as having a concentration of 0.0 are below the detection limits of the analyte.

3.3 N_2O Distribution

At each harbour station, depth and season (and their interaction) significantly impacted N_2O saturation (two-way ANOVA, $\alpha = 0.05$, *degree of freedom (d.f.)* = 59). At 2 m, N_2O saturation was observed to be below 100% at all stations in July 2022 (**Figure 5** and **Figure 6**) and at stations KR1, C10, and C08 in October 2022. In February and April 2023 N_2O saturation in the harbour was above 100% through the water column except in KR1 surface waters. The maximum N_2O concentrations were observed in the subhalocline. Among the subhalocline observations the maximum N_2O concentrations (reaching over 170%) were observed at the base of the Hells Gates sill at station C10 in October 2022.

All endmember N_2O concentrations were undersaturated in July 2022. In October, stations KR1 and HG3 were observed to be approx. 100% saturated but N_2O at station GR1 was undersaturated. In February and April 2023 N_2O concentrations were supersaturated at all endmember stations. There were statistically significant linear correlations between N_2O saturation and salinity ($r = 0.494$; $p = 5.5 \times 10^{-7}$, $n = 92$), temperature ($r = 0.391$; $p = 1.2 \times 10^{-4}$, *d.f.* = 90), DO concentration ($r = -0.563$; $p = 5.2 \times 10^{-9}$, *d.f.* = 90), and nitrate concentration ($r = 0.559$; $p = 6.9 \times 10^{-9}$, *d.f.* = 90) in the harbour stations (**Figure 7**). The correlation between N_2O saturation and the TAN concentration however was not statistically significant ($r = 0.174$; $p = 0.31$, *d.f.* = 34).

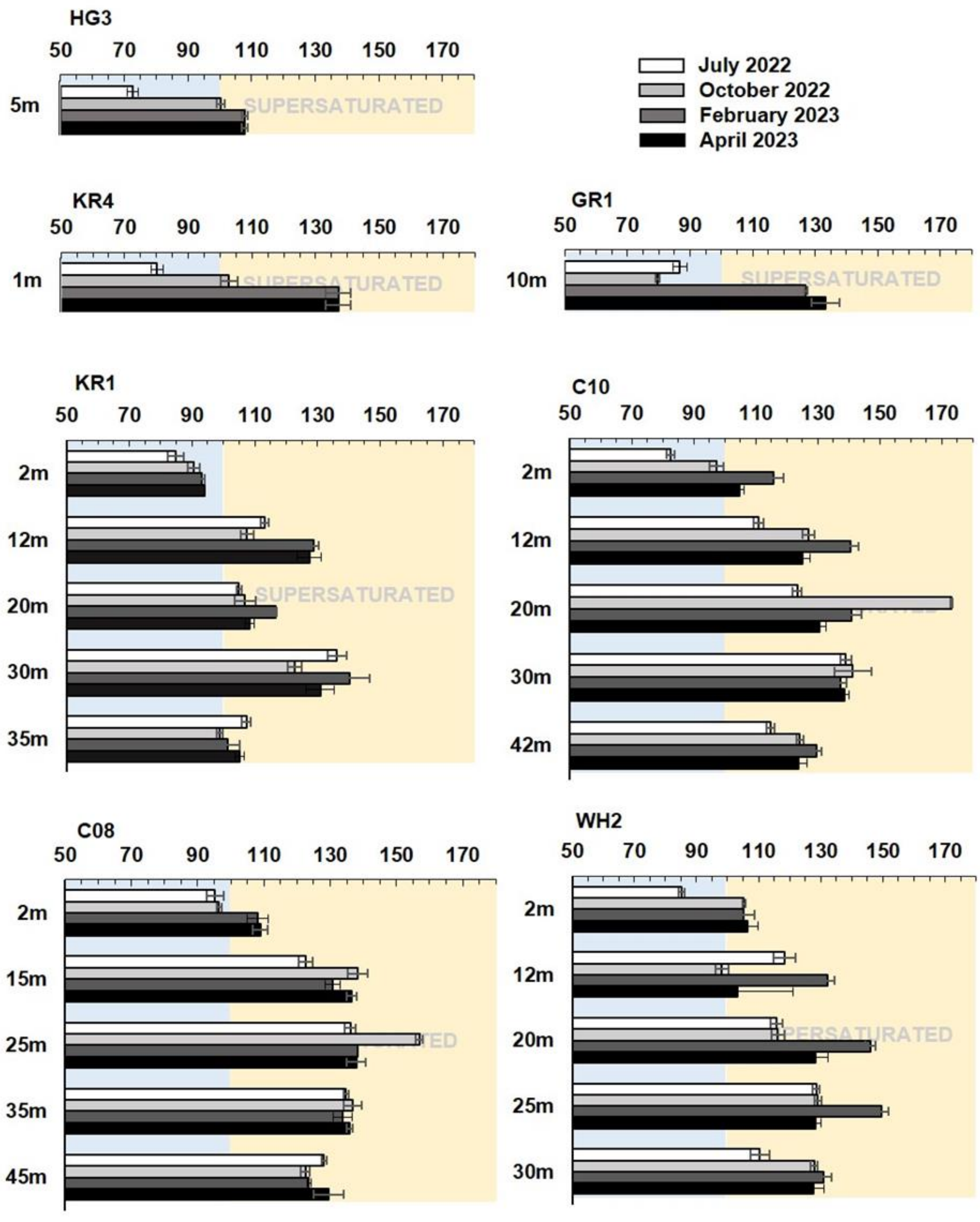

295 **Figure 5: Mean (± standard error) N_2O % saturation observed at each sampling station, with depth, and across seasons. Note that a red dashed line indicating 100% at the time of sampling has been placed on each panel for reference.**

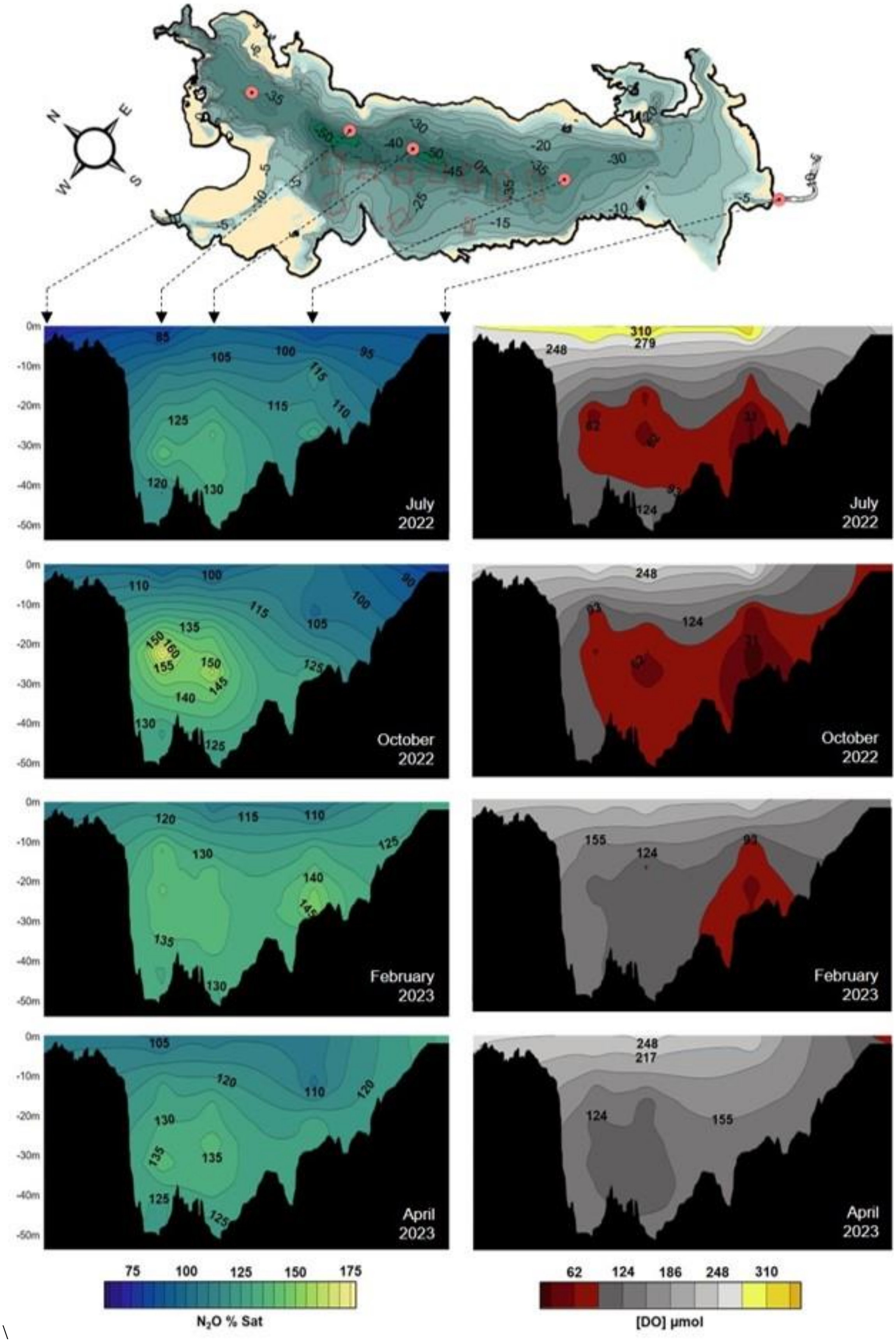

\

Figure 6: Contour plots of mean N_2O % saturation (left column) and mean DO concentration in units of µmol (right column) observed at stations HG3, C10, C08, WH2, and GR1 from July 2022 to April 2023. Red shaded areas on the DO plots indicate low oxygen concentrations (< 93 µmol). Relative positions of the stations are shown on the top left panel. Y-axis displays depth in metres relative to mean sea level.

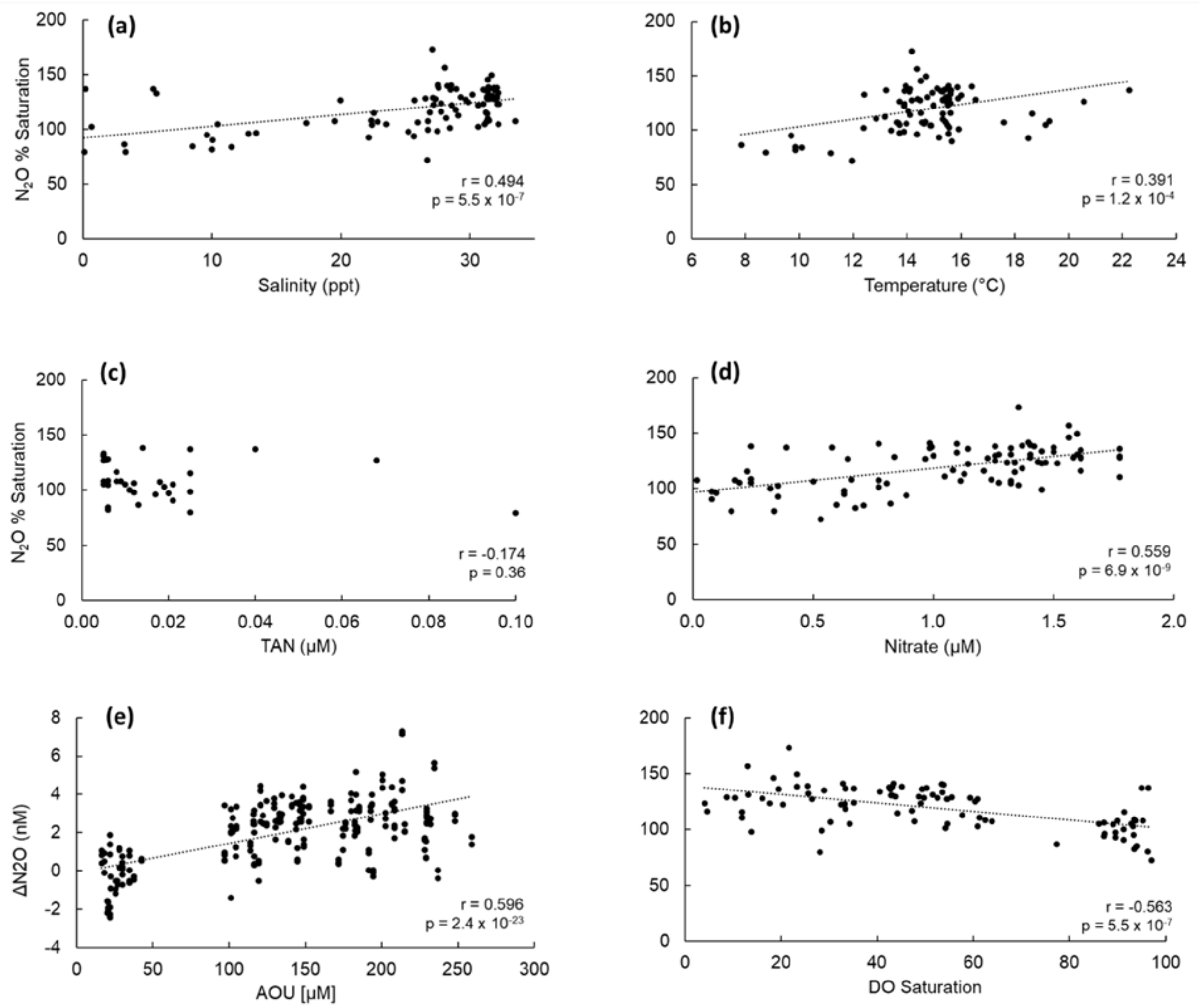

Figure 7: Correlation between N_2O % saturation observed across the harbour and a) Salinity, b) Temperature, c) Total Ammoniacal Nitrogen (TAN) concentration, d) Nitrate concentration. The correlation between AOU [μM] and ΔN_2O [nM] is shown in panel e). The relationship between N_2O % saturation and DO % saturation is shown in panel f) . Pearson correlation coefficients (r) and their associated p value are shown in each panel.

3.4 N_2O Air/Sea and Diapycnal Fluxes

Atmospheric N_2O mole fractions measured at Kinnaook / Cape Grim Air Pollution Station (*see* **Figure 1**) were observed to increase from 334.7 ppb in July 2022 to 335.9 ppb in February 2023. The April 2023 atmospheric N_2O mole fraction was slightly lower than that observed in February 2023 at 335.6 ppb. Average (± std. dev.) wind speeds were observed to be 6.6 (± 3.7) m sec^{-1} in July, 5.6 (± 2.5) m sec^{-1} in October, 6.3 (± 3.4) m sec^{-1} in February, and 6.4 (± 4.0) m sec^{-1} in April.

Estimated N_2O air/sea flux in the main harbour stations (KR1, C10, C08, WH2) ranged from -12.88 (± 6.00) μmol N_2O m^{-2} day^{-1} at C10 in July 2022 (negative sign indicates absorption of N_2O into the surface waters from the atmosphere) to 7.31 (± 3.43) μmol N_2O m^{-2} day^{-1} at the same station in February 2023 (using the "High" K_{600} estimator from **Raymond and Cole (2001)**; *see* **Table 2**)

Station KR1 was always observed to be a site of atmospheric N_2O uptake and was every non-endmember station in July 2022. Near the head of the system, station WH2 was observed to be a net source of N_2O to the atmosphere from October 2022 to April 2023, and stations C10 and C08 (positioned above the deepest basins) were net sources in February 2023 and April 2023.

Estimated diapycnal fluxes (± std. dev.) using local buoyancy frequencies showed a consistent upwards movement of N_2O from the subhalocline to surface layers with the smallest fluxes observed in July 2022 (49 ± 2.3 nmol N_2O m^{-2} day^{-1} at C08) and largest fluxes observed in October 2022 (up to 1308 nmol N_2O m^{-2} day^{-1} at WH2) and February 2023 (up to 1200 ± 47.3 nmol N_2O m^{-2} day^{-1} at C10) see **Table 3**. Patterns in the size of the diapycnal flux generally reflected the patterns of N_2O % saturation with the largest fluxes occurring in October 2022 during the periods of greatest N_2O % saturation. Overall the magnitude of the estimated diapycnal fluxes was smaller than estimated air/sea fluxes.

Table 2: Estimated sea-to-air N_2O flux (mean μmol N_2O m^{-2} day^{-1} ± std. dev.) of the main harbour stations using calculations presented in Bange et al. (2019) and Zhang et al. (2020) and a range of k_{600} parameterisations from Wanninkhof (2014; W_{2014}), Raymond and Cole (2001; RC_{Low}, RC_{Mid}, and RC_{High}), and Nightingale (2000; N_{2000}). Positive values indicate the flux of N_2O from the harbour water to the atmosphere. Negative values (shown in with bold text) indicate flux of N_2O from the atmosphere into the harbour water. Estimated Gordon River Flow and Mean (20 day) Gordon Above Dennison (GAD)Stream Gauge are also shown for each month as well as the Pearson Correlation and associated p-values between flow metrics, rainfall, and air/sea flux (and surface water % saturation).

Station	K_{600}	Jul 2022 μmol N_2O m^{-2} day^{-1}	Oct 2022 μmol N_2O m^{-2} day^{-1}	Feb 2023 μmol N_2O m^{-2} day^{-1}	Apr 2023 μmol N_2O m^{-2} day^{-1}	Gordon Flow vs Surface Flux	GAD Flow vs Surface Flux	GAD Flow vs % N_2O Sat.	Rainfall vs Surface Flux
KR1	RC_{High}:	**-11.07 ± 5.17**	**-04.01 ± 1.77**	**-03.30 ± 1.54**	**-03.17 ± 1.66**				
	RC_{Mid}:	**-08.45 ± 4.42**	**-03.19 ± 1.59**	**-02.55 ± 1.34**	**-02.44 ± 1.41**				
	RC_{Low}:	**-04.69 ± 3.17**	**-01.93 ± 1.27**	**-01.46 ± 0.99**	**-01.38 ± 0.99**	$r = -0.8316$, $p = 7.5 \times 10^{-4}$	$r = -0.8624$, $p = 3.1 \times 10^{-4}$	$r = -0.8726$, $p = 2.1 \times 10^{-4}$	$r = 0.5577$, $p = 0.060$
	N_{2000}:	**-0.85 ± 0.31**	**-0.30 ± 0.08**	**-0.25 ± 0.09**	**-0.24 ± 0.11**				
	W_{2014}:	**-0.78 ± 0.25**	**-0.27 ± 0.05**	**-0.23 ± 0.07**	**-0.22 ± 0.09**				
C10	RC_{High}:	**-12.88 ± 6.00**	**-01.21 ± 0.53**	07.31 ± 3.43	02.60 ± 1.36				
	RC_{Mid}:	**-09.83 ± 5.14**	**-00.96 ± 0.48**	05.65 ± 2.98	02.00 ± 1.16				
	RC_{Low}:	**-05.46 ± 3.68**	**-00.58 ± 0.38**	03.22 ± 2.19	01.13 ± 0.81	$r = -0.8298$, $p = 8.4 \times 10^{-4}$	$r = -0.9091$, $p = 4.2 \times 10^{-5}$	$r = -0.8795$, $p = 1.6 \times 10^{-4}$	$r = 0.2751$, $p = 0.387$
	N_{2000}:	**-0.99 ± 0.36**	**-0.09 ± 0.02**	0.67 ± 0.23	0.20 ± 0.09				
	W_{2014}:	**-0.91 ± 0.29**	**-0.08 ± 0.02**	0.61 ± 0.18	0.18 ± 0.07				
C08	RC_{High}:	**-03.50 ± 1.63**	**-01.69 ± 0.74**	04.08 ± 1.91	04.57 ± 2.40				
	RC_{Mid}:	**-02.67 ± 1.40**	**-01.34 ± 0.67**	03.15 ± 1.66	03.52 ± 2.03				
	RC_{Low}:	**-01.49 ± 1.00**	**-0.81 ± 0.53**	01.80 ± 1.22	01.98 ± 1.43	$r = -0.8547$, $p = 3.97 \times 10^{-4}$	$r = -0.8804$, $p = 1.6 \times 10^{-4}$	$r = -0.8447$, $p = 5.4 \times 10^{-4}$	$r = 0.1846$, $p = 0.566$
	N_{2000}:	**-0.27 ± 0.10**	**-0.12 ± 0.03**	0.31 ± 0.11	0.35 ± 0.15				
	W_{2014}:	**-0.25 ± 0.08**	**-0.11 ± 0.02**	0.29 ± 0.08	0.32 ± 0.13				
WH2	RC_{High}:	**-10.88 ± 5.06**	02.63 ± 1.15	02.40 ± 1.13	03.50 ± 1.84				
	RC_{Mid}:	**-08.30 ± 4.34**	02.09 ± 1.04	01.85 ± 0.98	02.69 ± 1.56				
	RC_{Low}:	**-04.61 ± 3.11**	01.26 ± 0.83	01.06 ± 0.72	01.52 ± 1.09	$r = -0.8071$, $p = 1.51 \times 10^{-3}$	$r = -0.8269$, $p = 9.1 \times 10^{-4}$	$r = -0.8077$, $p = 1.5 \times 10^{-3}$	$r = 0.6316$, $p = 0.028$
	N_{2000}:	**-0.84 ± 0.30**	0.19 ± 0.05	0.19 ± 0.06	0.27 ± 0.12				
	W_{2014}:	**-0.77 ± 0.24**	0.17 ± 0.03	0.17 ± 0.05	0.25 ± 0.10				
Gordon River Flow (m^3 sec^{-1})		383.6 ± 38.9	360.3 ± 54.1	342.6 ± 74.6	324.3 ± 26.6	-	-	-	-
GAD Flow (m^3 sec^{-1})		107.6 ± 15.9	73.7 ± 12.1	38.8 ± 5.1	30.5 ± 2.2	-	-	-	-

Table 3: Estimated diapycnal N_2O flux (nmol N_2O m^{-2} day^{-1} ± std. dev.) calculated form local buoyancy frequencies from 20 m to 2 m within the main harbour stations Positive values indicate the flux of N_2O from the basin water (20 m) to the surface lens (2m).

Station	July 2022 nmol N_2O m^{-2} day^{-1}	October 2022 nmol N_2O m^{-2} day^{-1}	February 2023 nmol N_2O m^{-2} day^{-1}	April 2023 nmol N_2O m^{-2} day^{-1}
KR1	80 ± 3.5	282 ± 17.7	992 ± 12.9	395 ± 8.6
C10	140 ± 4.5	1,200 ± 47.3	1,040 ± 65.3	454 ± 16.2
C08	49 ± 2.3	782 ± 12.1	778 ± 37.4	348 ± 18.6
WH2	117 ± 4.0	125 ± 2.8	1,308 ± 67.8	240 ± 18.0

4. Discussion

Our study is the first to report on N_2O distribution and air/sea flux from an Australasian fjord-like estuary. We set out to investigate how N_2O concentrations varied along horizontal and depth gradients; how N_2O concentrations and estimated surface water emissions vary seasonally; how N_2O concentrations vary with freshwater inputs; and whether the relationship between AOU and ΔN_2O could help clarify the primary mechanism for N_2O generation in this system. We used surface water observations, local wind speed (from Cape Sorell weather station) and atmospheric N_2O mole fractions (from Cape Grimm; **Figure 1**) to estimate N_2O air/sea flux (based on **Zhang *et al.*, 2010** and **Bange *et al.*, 2019**) and found that Macquarie Harbour functions as both a site of atmospheric uptake and emission of N_2O. Most harbour stations were estimated to be removing atmospheric N_2O in July and October 2022 (when river flow was greater) and emitting N_2O into the atmosphere in February and April 2023 (during low river flow periods; *see* **Figure 8** and **Table 2)**. Pearson correlations show that when freshwater flow is high N_2O air/sea flux is negative (indicating uptake from the atmosphere) and when freshwater flow is low N_2O air/sea flux is positive (**Table 2**). Our observations highlight that freshwater flow is a key driver of N_2O emissions in this estuary. In addition, Gordon River flow is heavily influenced by hydroelectric dam release (up to ~28% of the flow in July 2023). Rainfall in the catchment area may offset the effects of dam release, but our observations did not capture this as rainfall itself was not significantly correlated with N_2O concentrations or air/sea flux.

The river endmember concentrations of N_2O were often observed to be undersaturated, as observed in the South Platte River Basin, USA, **McMahon and Dennehy (1999)**; Neuse River Estuary, USA, **Stow *et al.*, (2005)**; headwater streams, Ontario, Canada, **Baulch *et al.*, (2011)**; and Upper Mara River Basin, Kenya, **Mwanke *et al.*, (2019).** Our observations of river endmember N_2O concentrations were similar to the lower end of the concentrations reported in **McMahon and Dennehy (1999)** (approx. 80% saturation), but not as low as those reported Jackson Creek, Ontario, Canada in **Baulch *et al.*, (2011)**, where some observations reached <20% saturation. N_2O undersaturation in those systems was attributed to complete denitrification (use of N_2O as a terminal electron acceptor by denitrifiers) in streams with high DOC loads, low DO, and low NO_3^- concentrations. It should also be noted that up to 28% of the estimated Gordon River flow was found to be associated with flow through the Gordon Above Dennison stream gauge (a proxy for hydroelectric dam/reservoir release to the Gordon River). Boreal reservoirs have been shown to be net sinks of atmospheric N_2O (**Hendzel *et al.*, 2005**) which was attributed to increased N_2O demand to drive complete denitrification. There is good reason to believe that N_2O may be scavenged in the Gordon and King Rivers as well because they do often have high DOC concentrations, high water column DO demand (**Maxey *et al.*, 2020**), and low DO concentrations in near the stream bed (**Maxey *et al.*, 2022**).

Below the estuary's predominately freshwater surface lens, the fjord-like morphology drives suboxic conditions like those observed in the subhalocline waters at station WH2 in October 2022 (*see* **Figure 3; Hartstein *et al.*, 2019; Maxey *et al.*, 2020, 2022**). While these conditions do not always persist, DO concentrations below 31 µM have been observed to occur more than 30% of the time up estuary, specifically at station WH2 (**Maxey *et al.*, 2022**). In the low DO sub-halocline layers of the harbour we observed the maximum N_2O concentrations (**Figure 5** and **Figure 6**). Subhalocline N_2O saturation was observed to generally range from approx. 110% to 170% with the highest values observed within the deeper basins near the foot of the sill (stations C10 and C08; **Figure 6**).

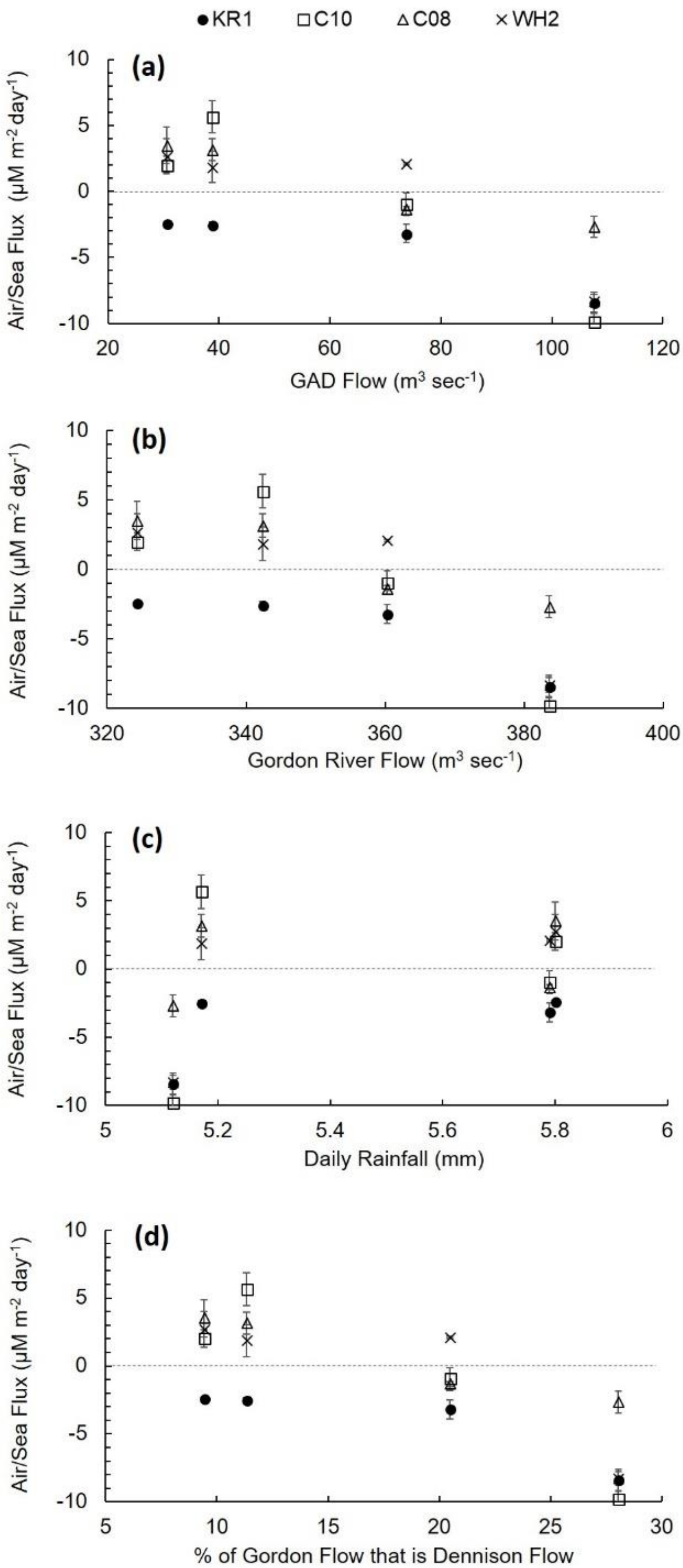

Figure 8: Mean Air/Sea Flux (μM m^{-2} day^{-1}) versus a) Gordon above Dennison River flow (m^3 day^{-1}), b) estimated Gordon River flow (m^3 day^{-1}), c) daily rainfall (mm) (20 day mean), and d) % of estimated Gordon River flow this is accounted for by the Gordon above Dennison River gauge (proxy for hydroelectric dam release). Error bars indicate ± 1 standard error.

In the harbour's subhalocline layer there is not enough light to support photosynthesis (**Hartstein *et al.*, 2019**; **Maxey *et al.*, 2017, 2020, and 2022**) and thus the main source of oxygen is advection from marine intrusions. N_2O producing microbes have been observed to populate this layer of the harbour (*see* **Da Silva *et al.*,**

2021 and **2022**) and our observations of supersaturated N_2O in these layers show that those microbes are active. Linear relationships between AOU and ΔN_2O (slope = 0.0154; r = 0.596; p = 2.4 x $10^{-23;}$ **Figure 7C**) and NO_3^- and N_2O saturation (r = 0.559; p = 6.9 x 10^{-9}; **Figure 7D**) indicate that N_2O production likely occurs primarily through the ammonia oxidation (nitrification) pathway (**Yoshinari, 1976; Walter *et al.*, 2004; Brase *et al.*, 2017**). Our observations are on the lower end of reported N_2O yield per mole O_2 consumed (see **Suntharalingam and Sarmiento, 2000; Brase *et al.*, 2017**) which may be an artefact of mixing and loss dynamics such as basin water DO recharges from marine intrusions, and loss to aerobic respiration and the atmosphere. This suggests that some portion of subhalocline pelagic oxygen demand in the harbour can be attributed to nitrifying microbes (albeit at a much lower rate compared to aerobic respiration). **Ji *et al.*, (2020)** also observed similar relationships in the Saanich Inlet, a seasonally anoxic fjord-like estuary in British Columbia, but in that system anoxic conditions are more persistent (**Bourbonnais *et al.*, 2013; Manning *et al.*, 2010**) compared to Macquarie Harbour (**Maxey *et al.*, 2022**). Deep-water renewal / marine intrusions have been hypothesized to stimulate N_2O production in the Saanich Inlet (**Capelle *et al.*, 2018; Michiles *et al.*, 2019**; **Ji *et al.*, 2020**), and Baltic Sea (**Walter *et al.*, 2006**) and may also be stimulating it in Macquarie Harbour as well. In the Baltic Sea, **Walter *et al*. (2006)** and **Myllykangas *et al.* (2017)** observed enhanced N_2O production in areas receiving significant marine intrusions. Positive correlations between AOU and ΔN_2O observed in western Baltic Sea waters (**Walter *et al.*, 2006**) along with mean (11-year; 2006-2017) seasonal variations in DO and N_2O observed through the water column at the Boknis Eck Time-Series Station (Eckernförde Bay, Southwest Baltic Sea) indicate a tight coupling between DO supply and N_2O production (presumably by nitrification) / consumption (presumably by denitrification) pathways in that area (**Ma *et al.*, 2019**). The reintroduction of marine water on the upstream side of a dam in the Nakong River, South Korea was found to affect bottom water trapping (stagnation), DO conditions, N process rates, process specific gene abundances, and subsequently the fate of N in that system (**Huang *et al.*, 2024**). Marine intrusions primarily refresh the DO supply adjacent to the sill in Macquarie Harbour (near station C10). As we observed a positive correlation between AOU and ΔN_2O marine intrusions offer a possible explanation for the higher subhalocline N_2O concentrations observed in this part of the harbour (*see* **Figure 7E**).

One other possible pathway of water column N_2O production might be through denitrification as DO concentrations at WH2 in October 2022 approached single digits (3.1 µM). This station has the highest basin residence time compared the others used in this study. Low oxygen concentrations may also likely be found under the harbour's fish farms due to the aerobic respiration of farm debris (**Maxey *et al.* 2020**). Though whether denitrification functions as a production process or a loss process will depend upon the drivers of DO concentration (*i.e.* respiration rates, physical mixing, *etc.*) and may differ depending on the location of the basins in this system. It is likely the main driver of undersaturated N_2O concentrations in the Gordon River.

We conceptualize that during periods of high river flow, the surface water lens thickens and transports water undersaturated with N_2O quickly across the harbour surface and out of Hells Gates inlet. N_2O from the continuously oversaturated subhalocline water is entrained in the surface lens (diapycnal flux) and transported laterally and out of the system in its dissolved form. During periods of low river flow, the surface lens is thinner and residence times longer (**Andrewartha and Wild-Allen 2017; Maxey *et al.*, 2022**). We suspect that N_2O from the oversaturated subhalocline water then diffuses through the surface layer and is emitted into the atmosphere in its gaseous form (**Figure 9**). Our estimates of diapycnal flux indicate that the mass transport from subhalocline waters is smaller (~2x smaller) than the air/sea flux, supporting this idea. This conceptual model suggests that the harbour surface lens functions to capture both gaseous N_2O from the atmosphere and dissolved N_2O generated in the subhalocline layer and transport it to the ocean is its dissolved form during high flow periods (**Figure 9**).

This study focusing on characterizing N_2O dynamics at end-members and at stations through the harbour's longitudinal axis. Other areas of the harbour, most prominently the shallow embayments around the parameter of the system and the areas occupied by fin fish farms were not included here. Fin fish aquaculture can increase water column DO demand near the pens in this system (**Maxey *et al.*, 2020**), and introduces particulate organic material to the water. Whether this manifests in altered N cycling dynamics (especially DO sensitive processes like nitrification and denitrification) would be system specific and has never been described in this system. High particles loads have been shown to induce denitrification in normoxic waters *e.g.* **Wan et al., (2023)***;* **Frey et al., (2020)***;* **Codispoti et al., (2005)***;* **Nevison et al., (2003)***;* **Usui et al., (2001)***;* **Robinson et al., (1998)** so an N_2O sink might be present even under farms, even in more oxygenated basins. Future studies should investigate the impacts of fin fish aquaculture on DO and N_2O cycling.

One source of uncertainty in our approach is in using literature derived estimators for air/sea and diapycnal flux estimations. We also used literature derived k_{600} estimates from **Nightingale *et al.*, (2000)**, **Raymond and Cole (2001)**, and **Wanninkhof (2014)** to compute N_2O air/sea flux. Literature derived estimators of K_{600} and eddy diffusivity are commonly used when direct measurements are unavailable (**Tang *et al.*, 2024**; **Li *et al.* 2023; Murray *et al.* 2020**) but to reduce uncertainty these are ideally measure in situ. Likewise, we presented diapycnal flux estimates using turbulent eddy diffusivities from **Fer *et al.*, (2006)** which were not measured in Macquarie Harbour.

Previous work in Australian estuaries with pristine catchments (like Macquarie Harbour) has shown that many tend to function as a sink for atmospheric N_2O (**Maher *et al.*, 2016; Wells *et al.*, 2018**). Our study adds the caveat that water column / atmospheric exchange may also depend on factors controlling river flow in deeper stratified systems. Despite the advancements made to date, many of the deeper estuaries in Chile, Australia and New Zealand are lacking descriptions of N_2O exchange between the water column and atmosphere (*e.g.* Bathurst Harbour, Tasmania; fjords of South Island New Zealand; estuaries on Stewart Island New Zealand). Given that these systems have relatively pristine catchments they offer an opportunity to better understand natural fjord-like estuarine responses to the climate drivers of N_2O dynamics. Mesoscale climate oscillations (*i.e.* the Southern Annular Mode; SAM; North Atlantic Oscillation; NAO) have been shown to affect rainfall, river flow, and DO concentrations in this and other fjord-like estuaries (**Maxey *et al.*, 2022**; **Austin and Inall, 2002)**. In Western Tasmania, SAM in its positive phase results in increased orographic rainfall and a greater propensity for higher river flow, possibly tilting the source and sink balance to net N_2O uptake during these periods.

Climate change predictions for Tasmania's West Coast (which includes the Macquarie Harbour catchment) indicate that the region will experience a more extreme precipitation regime with increased winter precipitation and decreased summer precipitation (**Grose *et al.*, 2010; Bennett *et al.*, 2010**). If these future predictions result in more extreme seasonality in Gordon River flow, then the harbour may respond in kind with a larger variation in N_2O air / sea flux *i.e.* greater N_2O atmospheric uptake in winter and greater N_2O emission in summer. However, given that the river flow is somewhat regulated by the hydroelectric dam, our study suggests that flow regulation has the potential to augment harbour N_2O emissions. Releasing water during extreme low rainfall periods might allow N_2O slowly accumulating in subhalocline waters to be released in the exported surface lens. Fjord and fjord-like estuaries are defined by their strong stratification and sensitivity to freshwater inputs. With climate change, rainfall patterns are expected to become more extreme and thus alter the river flow, and subsequently N_2O source sink dynamics in these systems on a global scale. In systems that are expected to experience increasingly drier conditions they may shift from net sinks of N_2O to sources, and further perpetuate the accumulation of N_2O in the atmosphere.

It is well established that fjord and fjord-like estuaries are important sites of C burial (**Smith *et al.*, 2015; Bianchi *et al.*, 2018, 2020**). This study supports the idea that they can also be important sites of atmospheric N_2O removal and transport. Macquarie Harbour air/sea flux estimates are similar in magnitude to observations made in other stratified estuaries and enclosed seas such as the Reloncaví Estuary, Chile (**Yevenes *et al.*, 2017**) and Eckernförde Bay, Germany (**Ma *et al.*, 2019**) (**Table A1**). Macquarie Harbour, however, was observed to have lower fluxes of N_2O into the atmosphere than other river dominated, but not fjord-like, estuaries (Elbe River, Germany; **Schulz *et al.*, 2023**) including those on the Australian mainland's east coast (**Wells *et al.*, 2018**).

5. Conclusions

In summary, river flow, and specifically river flow driven by hydroelectric dam release, significantly affects both surface water N_2O concentrations and air/sea flux in Macquarie Harbour. Importantly, when river flow is low most of the harbour emits N_2O to the atmosphere. When river flow is high most of the harbour removes N_2O from the atmosphere, intercepts the diapycnal flux, and laterally exports this N_2O to the ocean in its dissolved form. N_2O is continually supersaturated below the halocline and the relationship between AOU and ΔN_2O and N_2O saturation and NO_3^- concentration indicates that the main N_2O generation process is likely nitrification. Climate change is predicted to result in wetter winter / drier summers for the Tasmanian West Coast, which may result in augmented N_2O air/sea fluxes. This work represents the first descriptions of N_2O spatiotemporal distribution, estimated air/sea flux, estimated diapycnal flux, and N_2O production pathways in this system.

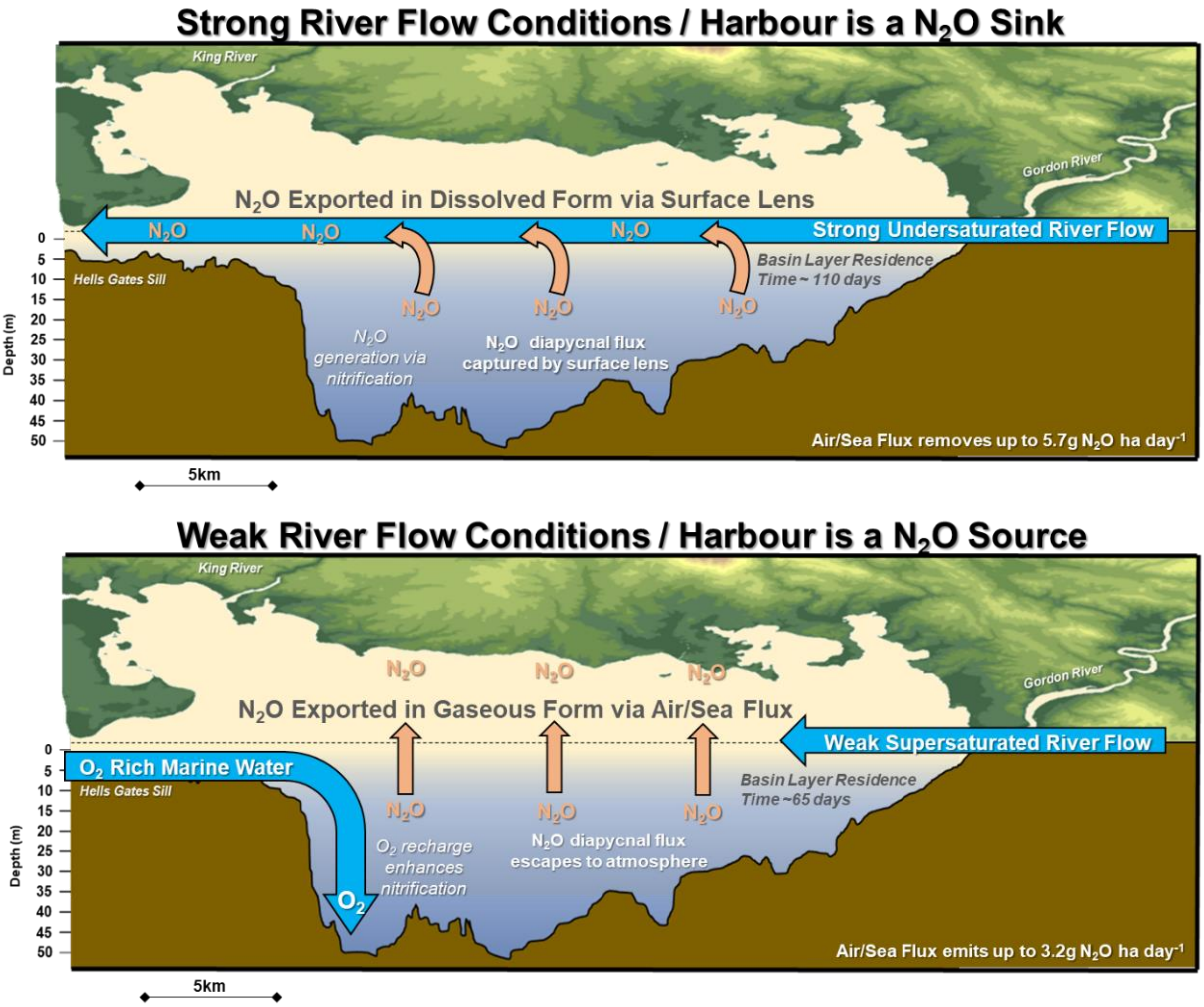

Figure 9: Conceptual model of Macquarie Harbour's N_2O dynamics. The top diagram depicts the capture of N_2O generated in the subhalocline during strong river flow conditions. Here N_2O is exported from the harbour in its dissolved form via undersaturated surface flows from the harbour to the ocean. The bottom diagram depicts the efflux of N_2O from the harbour surface during low flow conditions. Note that during these conditions the surface flows are weak and generally supersaturated with N_2O permitting its escape in gaseous form to the atmosphere.

6. Appendix

Table A1: N_2O fluxes and observed ranges of mean (± standard deviation) N_2O concentration / saturation from both fjord-like / river dominated estuaries around the globe and estuaries in Australia.

Location	System Type	Measurement Depth Range	Mean Sea-to-Air N_2O flux uMol N_2O m^{-2} day^{-1}	Min and Max Sea-to-Air N_2O flux uMol N_2O m^{-2} day^{-1}	Mean N_2O Concentration (and Saturation) nM N_2O (and %)	Min and Max N_2O Concentration (and Saturation) nM N_2O (and %)	Reference
Macquarie Harbour, Western Tasmania, Australia	Fjord-like Estuary	2m to 45m	-09.83 ± 0.67 to 05.65 ± 1.22	-10.82 to 7.73	11.7 ± 1.6 (121.8 ± 17.8)	7.87 to 17.12 (81 to 174)	*This Study*
Reloncaví Estuary, Chile	Fjord-like Estuary	0m to 5m	0.86 ± 2.28	-1.58 to 5.60	11.8 ± 1.70 (111 ± 18.3)	8.34 to 14.5 (80 to 140)	Yevenes *et al.*, 2017
Reloncaví Estuary, Chile	Fjord-like Estuary	10m to 200m	-	-	14.5 ± 1.73 (145 ± 17.7)	10.5 to 17.0 (11 to 170)	Yevenes *et al.*, 2017
Chiloé Interior Sea, Chile	Fjord-like Estuary	0m to 200m	1.08 ± 1.41	-0.18 to 3.19	12.6 ± 2.36 (121 ± 17.5)	8.81 to 21.1 (87 to 160)	Yevenes *et al.*, 2017
Europa Sound, Magellanic Region, Chile	Fjord-like Estuary	1m to 10m	-15.22 to -0.81	-	11.9 ± 5.7 to 12.7 ± 1.0	-	Farías *et al.*, 2018
Concepción Channel, Magellanic Region, Chile	Fjord-like Estuary	1m to 150m	0.69 to 7.70	-	13.6 ± 1.1 to 17.0 ± 0.02	-	Farías *et al.*, 2018
Sarmiento Channel, Magellanic Region, Chile	Fjord-like Estuary	1m to 10m	2.07 to 12.53	-	13.1 ± 0.1 to 16.5 ± 0.3	-	Farías *et al.*, 2018
Estero Peel, Magellanic Region, Chile	Fjord-like Estuary	1m to 10m	0.11 to 2.01	-	13.1 ± 0.2 to 13.5 ± 0.5	-	Farías *et al.*, 2018
Estero Calvo, Magellanic Region, Chile	Fjord-like Estuary	1m to 10m	0.04	-	13.9 ± 0.8	-	Farías *et al.*, 2018
Estero Amalia, Magellanic Region, Chile	Fjord-like Estuary	1m to 100m	-0.08	-	14.2 ± 1.7	-	Farías *et al.*, 2018
Estero las Montañas, Magellanic Region, Chile	Fjord-like Estuary	1m to 10m	-2.95	-	9.69 ± 1.6	-	Farías *et al.*, 2018
Smyth Channel, Magellanic Region, Chile	Fjord-like Estuary	1m to 300m	1.07 to 11.2	-	14.3 ± 0.4 to 16.0 ± 0.5	-	Farías *et al.*, 2018
Última Esperanza Sound, Magellanic Region, Chile	Fjord-like Estuary	1m to 10m	-3.7 to 10.4	-	12.1 ± 1.1 to 13.7 ± 0.07	-	Farías *et al.*, 2018
Almirante Montt Gulf, Magellanic Region, Chile	Fjord-like Estuary	1m to 150m	15.6	-	21.0 ± 5.7	-	Farías *et al.*, 2018
Kirke Channel, Magellanic Region, Chile	Fjord-like Estuary	1m to 10m	0.12 to 8.19	-	13.3 ± 0.1 to 15.4 ± 0.4	-	Farías *et al.*, 2018
Union Channel, Magellanic Region, Chile	Fjord-like Estuary	1m to 10m	22.1	-	16.7 ± 0.8	-	Farías *et al.*, 2018
Union Sound, Magellanic Region, Chile	Fjord-like Estuary	1m to 10m	2.86	-	14.8 ± 0.8	-	Farías *et al.*, 2018
Western Magellan Strait, Magellanic Region, Chile	Fjord-like Estuary	1m to 10m	143	-	15.71	-	Farías *et al.*, 2018
Eastern Magellan Strait, Magellanic Region, Chile	Fjord-like Estuary	1m	36.3	-	16.4	-	Farías *et al.*, 2018
San Gregorio Cape, Magellanic Region, Chile	Fjord-like Estuary	1m	24.8	-	12.07	-	Farías *et al.*, 2018
Otway Center Sound, Magellanic Region, Chile	Fjord-like Estuary	1m	35.5	-	11.4	-	Farías *et al.*, 2018
Magdalena North Channel, Magellanic Region, Chile	Fjord-like Estuary	1m	-0.22	-	11.4	-	Farías *et al.*, 2018
Chasco Sound, Magellanic Region, Chile	Fjord-like Estuary	1m	6.81	-	16.01	-	Farías *et al.*, 2018
Cockburn West Channel, Magellanic Region, Chile	Fjord-like Estuary	1m	6.18	-	14.47	-	Farías *et al.*, 2018
Saanich Inlet, British Columbia, Canada	Fjord-like Estuary	10m to 200m	2.3 ± 2.5 to 3.9 ± 2.9	-	14.7	<0.5 to 37.4	Capelle *et al.*, 2018
Saanich Inlet, British Columbia, Canada	Fjord-like Estuary	Surface to 110m	11.3 to 20.4	-	-	-	Cohen 1978
Elbe River Estuary, Germany	Well-Mixed River Dominated Estuary	1.2m	-	26.0 ± 23.5 to 100.7 ± 101.2	-	(161 ± 53.6) to (243 ± 141.6)	Schulz *et al.* 2023
Eckernförde Bay, Boknis Eck Time Series Station, Baltic Sea, Germany	Enclosed Sea	1m to 25m	3.5 ± 12.4	-19.0 to 105.7	(111± 30)	(56 to 314)	Ma *et al.*, 2019
Eckernförde Bay, Boknis Eck Time Series Station, Baltic Sea, Germany	Enclosed Sea	1m to 25m	-	-	10 to 17	-	Walter *et al.*, 2006
Baltic Sea, Germany	Enclosed Sea	110m	5 -11	-	14 to 1523	-	Rönner 1983

Gotland Basin, Baltic Sea, Germany	Enclosed Sea	90m	-	-	13	0 to 126 (0 to 450)	Brettar and Rheinheimer 1991
Northwest Shelf, Black Sea	Enclosed Sea	-	1.6 to 4.4	-	6.5 to 8	-	Amouroux *et al.*, 2002
Deep Basin, Black Sea	Enclosed Sea	70m	3.1 to 5.2	-	7.5 to 10.2	-	Amouroux *et al.*, 2002
Cariaco Basin, Venezuela	Coastal Basin	Surface to 400m	-	-	4.4 to 5.5	-	Hashimoto *et al.*, 1983
Guadalquivir Estuary, Gulf of Cadiz, Spain	River Dominated Estuary	2m	18.7 ± 33.6	-	20.6 ± 24.3	-	Sierra *et al.*, 2020
Guadalquivir Estuary, Gulf of Cadiz, Spain	River Dominated Estuary	2m	0.3 ± 0.5	-	6.7 ± 0.4	-	Sierra *et al.*, 2020
Guadalquivir Estuary, Gulf of Cadiz, Spain	River Dominated Estuary	2m	0.9 ± 21.6	-	7.3 ± 15.4	-	Sierra *et al.*, 2020
Noosa River Estuary, Eastern Australia	River Dominated Estuary	0.5m to 9.6m	-14.24 ± 14.02	-57.72 to 22.20	6.99 ± 0.43 (97 ± 2.2)	5.92 to 7.95 (90 to 103)	Wells *et al*., 2018
Mooloolah River Estuary, Eastern Australia	River Dominated Estuary	0.5m to 6.8m	-7.33 ± 7.25	-48.76 to 16.31	6.74 ± 0.64 (97 ± 3.8)	5.19 to 7.71 (82 to 112)	Wells *et al*., 2018
Maroochy River Estuary, Eastern Australia	River Dominated Estuary	0.5m to 8.2m	51.33 ± 55.3	-34.94 to 179.64	8.4 ± 1.50 (113 ± 16.7)	6.07 to 12.93 (92 to 163)	Wells *et al*., 2018
Pine River Estuary, Eastern Australia	River Dominated Estuary	0.5m to 10.1m	17.10 ± 39.44	-33.22 to 145.50	7.1 ± 0.76 (102 ± 6.24)	6.05 to 8.57 (93 to 117)	Wells *et al*., 2018
Brisbane River Estuary, Eastern Australia	River Dominated Estuary	0.5m to 23.9m	209.54 ± 143.59	15.42 to 662.62	9.8 ± 1.36 (133 ± 9.9)	6.75 to 12.75 (105 to 158)	Wells *et al*., 2018
Middle Reach, Brisbane River Estuary, Eastern Australia	River Dominated Estuary	Surface	14.5 ± 1.19	5.4 ± 0.34 to 25.2 ± 1.87	-	13.1 to 17.9 (160 to 250)	Sturm *et al.*, 2017
Lower Reach, Brisbane River Estuary, Eastern Australia	River Dominated Estuary	Surface	6. ± 0.51	3.7 ± 0.85 to 9.1 ± 1.19	-	9.2 to 12.7 (125 to 410)	Sturm *et al.*, 2017
Oxley Creek, Eastern Australia	River Dominated Estuary	2.1m to 13.1m	210.59 ± 60.23	91.54 to 280.16	11.7 ± 1.34 (156 ± 19.7)	9.65 to 14.89 (139 to 199.7)	Wells *et al.*, 2017
Nerang River Estuary, Eastern Australia	River Dominated Estuary	0.5m to 6.8m	-0.62 ± 20.87	-67.98 to 45.92	6.73 ± 0.43 (100 ± 4.3)	5.99 to 7.79 (88 to 109)	Wells *et al*., 2018
Logan River Estuary, Eastern Australia	-	0.5m to 14.4m	110.00 ± 153.55	-54.48 to 796.00	9.3 ± 2.36 (127 ± 27.5)	5.54 to 14.8 (81 to 191)	Wells *et al*., 2018
Albert River Estuary, Eastern Australia	-	1.1m to 15.7m	90.05 ± 73.32	-9.50 to 264.25	10.10 ± 2.24 (131 ± 29.8)	7.32 to 15.1 (98 to 205)	Wells *et al*., 2018
Darwin Creek, Australia	Mangrove Creek	~1m	-0.12	-	6.3 (98.9)	6.0 to 6.8 (95 to 104)	Maher *et al.*, 2016
Hinchinbrook Creek, Australia	Mangrove Creek	~1m	-3.43	-	6.1 (83.3)	5.6 to 6.8 (75 to 91)	Maher *et al.*, 2016
Melbourne Creek, Australia	Mangrove Creek	~1m	-1.33	-	7.9 (96.6)	6.9 to 9.1 (86 to 115)	Maher *et al.*, 2016
Morton Bay Creek, Australia	Mangrove Creek	~1m	-3.19	-	5.1 (77.4)	3.4 to 6.6 (50 to 105)	Maher *et al.*, 2016
Seventeen Seventy Creek, Australia	Mangrove Creek	~1m	-1.75	-	7.7 (94.3)	7.1 to 8.9 (88 to 106)	Maher *et al.*, 2016
Brisbane River, Australia	-	-	-	-	(285)	(135 to 435)	Musenze *et al.*, 2014
Coffs Creek, Australia	-	-	-	-	(219 ± 37)	(53 to 386)	Reading *et al.*, 2017
Coffs Creek, Australia	-	-	-	-	(266.5 ± 128)	(86 to 678)	Reading *et al.*, 2020
Boambee Creek, Australia	-	-	-	-	(197.1 ± 75)	(87 to 329)	Reading *et al.*, 2020
Bonville Creek, Australia	-	-	-	-	(183.7 ± 65)	(78 to 310)	Reading *et al.*, 2020
Pine Creek, Australia	-	-	-	-	(194.1 ± 65)	(79 to 382)	Reading *et al.*, 2020
Yarra River, Australia	Salt Wedge Estuary	-	-	-	(135.9 ± 31)	-	Tait *et al.*, 2017

7. Acknowledgments

We would like to thank GEOMAR for providing the facilities and training (thank you Lea, Florian, and Chukwudi) required to analyse N_2O samples. We want to thank Torsten and Leonie Schwoch for their sampling assistance and tireless vessel operation on the Harbour. We want to thank the ADS Environmental Services *Sdn. Bhd.* technical staff for helping to collect portions of this dataset (Grace, Shukry, Atika, Chance, Gene, and Azza). We would also like to thank our families for supporting our long days away from home. This research has been supported by internal funding from ADS Environmental Services, Swinburne University of Technology student travel grant, and GEOMAR. We have used some of the data available in the MEMENTO database. The MEMENTO database is administered by the Kiel Data Management Team at GEOMAR Helmholtz Centre for Ocean Research Kiel. The database is accessible through the MEMENTO webpage: https://memento.geomar.de.

8. Data Availability

This data set is available upon request

9. Author Contributions

Johnathan Daniel Maxey – *Conceptualization, Field Collection, Analytical Methodology, Data Analysis, Writing – Original Draft, Writing – Review & Editing*

Neil David Hartstein – *Conceptualization, Field Collection, Analytical Guidance, Writing – Review & Editing, Funding*

Hermann W. Bange – *Conceptualization, Analytical Methodology, Data Analysis, Writing – Review & Editing*

Moritz Müller – *Conceptualization, Field Collection, Analytical Guidance, Writing – Review & Editing*

10. Competing Interests

HWB serves on the editorial board for Biogeosciences. The authors declare that they have no other conflicts of interest.

11. References

Borges, A. V., Delille, B., Schiettecatte, L. S., Gazeau, F., Abril, G., and Frankignoulle, M.: Gas transfer velocities of CO2 in three European estuaries (Randers Fjord, Scheldt, and Thames). Limnology and Oceanography, 49(5), 1630-1641, 2004. DOI: 10.4319/lo.2004.49.5.1630

Acuña-González, J. A., Vargas-Zamora, J. A., and Córdoba-Muñoz, R.: A snapshot view of some vertical distributions of water parameters at a deep (200 m) station in the fjord-like Golfo Dulce, embayment, Costa Rica. Revista de Biología Tropical, 54(1), 193-200, 2006. ISSN: 0034-7744

Amouroux, D., Roberts, G., Rapsomanikis, S., and Andreae, M. O.: Biogenic gas (CH_4, N_2O, DMS) emission to the atmosphere from near-shore and shelf waters of the north-western Black Sea. Estuarine, Coastal and Shelf Science, 54(3), 575-587, 2002. DOI: 10.1006/ecss.2000.0666

Andrewartha, J. and Wild-Allen, K.: CSIRO Macquarie Harbour Hydrodynamic and Oxygen Tracer Modelling. Progress report to FRDC 2016/067 Project Steering Committee, 2017.

Arneborg, L., Janzen, C., Liljebladh, B., Rippeth, T. P., Simpson, J. H., and Stigebrandt, A.: Spatial variability of diapycnal mixing and turbulent dissipation rates in a stagnant fjord basin. Journal of Physical Oceanography, 34(7), 1679-1691, 2004. DOI: 10.1175/1520-0485(2004)034<1679:SVODMA>2.0.CO;2

Austin, W. E., and Inall, M. E.: Deep-water renewal in a Scottish fjord: temperature, salinity and oxygen isotopes. Polar Research, 21(2), 251-257, 2002. DOI: 10.3402/polar.v21i2.6485

Bange, H. W., Rapsomanikis, S., and Andreae, M. O.: Nitrous oxide in coastal waters. Global Biogeochemical Cycles, 10(1), 197-207, 1996. DOI: 10.1029/95GB03834.

Bange, H. W.: Nitrous oxide and methane in European coastal waters. Estuarine, Coastal and Shelf Science, 70(3), 361-374, 2006. DOI: 10.1016/j.ecss.2006.05.042

Bange, H. W., Bell, T. G., Cornejo, M., Freing, A., Uher, G., Upstill-Goddard, R. C., and Zhang, G. L.: MEMENTO: A proposal to develop a database of marine nitrous oxide and methane measurements. Environmental Chemistry, 6, 195-197, 2009. DOI: 10.1071/en09033.

Bange, H. W., Sim, C. H., Bastian, D., Kallert, J., Kock, A., Mujahid, A., and Müller, M.: Nitrous oxide (N_2O) and methane (CH_4) in rivers and estuaries of northwestern Borneo. Biogeosciences, 16(22), 4321-4335, 2019. DOI: 10.5194/bg-16-4321-2019

Bange, H. W., Mongwe, P., Shutler, J. D., Arévalo-Martínez, D. L., Bianchi, D., Lauvset, S. K., Liu, C., Löscher, C. R., Martins, H., Rosentreter, J. A., Schmale, O., Steinhoff, T., Upstill-Goddard, R. C., Wanninkhof, R., Wilson, S. T., and Xie, H.: Advances in understanding of air–sea exchange and cycling of greenhouse gases in the upper ocean, Elementa: Science of the Anthropocene, 12, 2024. DOI: 10.1525/elementa.2023.00044

Bastian, D.: N_2O und CH_4 Verteilung in Ästuaren und Flüssen im Nordwesten von Borneo, 2017. BSc thesis, Kiel University, Kiel, 50 pp., 2017.

Baulch, H. M., Schiff, S. L., Maranger, R., and Dillon, P. J.: Nitrogen enrichment and the emission of nitrous oxide from streams. Global Biogeochemical Cycles, 25(4), 2011. DOI: 10.1029/2011GB004047

Beaulieu, J. J., Shuster, W. D., and Rebholz, J. A.: Controls on gas transfer velocities in a large river. Journal of Geophysical Research: Biogeosciences, 117(G2), 2012. DOI: 10.1029/2011JG001794

Bennett, J. C., Ling, F. L. N., Graham, B., Grose, M. R., Corney, S. P., White, C. J., Holz, G. K., Post, D. A., Gaynor, S. M. and Bindoff, N. L.: Climate Futures for Tasmania: water and catchments technical report.

Antarctic Climate & Ecosystems Cooperative Research Centre, Hobart, Tasmania, 2010. ISBN: 978-1-921197-06-8

Bianchi, T. S., Cui, X., Blair, N. E., Burdige, D. J., Eglinton, T. I., and Galy, V.: Centers of organic carbon burial and oxidation at the land-ocean interface. Organic Geochemistry, 115, 138-155, 2018. DOI: 10.1016/j.orggeochem.2017.09.008

Bianchi, T. S., Arndt, S., Austin, W. E., Benn, D. I., Bertrand, S., Cui, X., Faust, J., Koziorowska-Makuch, K., Moy, C., Savage, C., Smeaton, C., Smith, R., and Syvitski, J.: Fjords as aquatic critical zones (ACZs). Earth-Science Reviews, 203(103145), 2020. DOI: 10.1016/j.earscirev.2020.103145

Brase, L., Bange, H. W., Lendt, R., Sanders, T., and Dähnke, K.: High resolution measurements of nitrous oxide (N_2O) in the Elbe estuary. Frontiers in Marine Science, 4(162), 2017. DOI: 10.3389/fmars.2017.00162

Breider, F., Yoshikawa, C., Makabe, A., Toyoda, S., Wakita, M., Matsui, Y., Kawagucci, S., Fujiki, T., Harada, N. and Yoshida, N.: Response of N_2O production rate to ocean acidification in the western North Pacific. Nature Climate Change, 9(12), 954-958, 2019. DOI: 10.1038/s41558-019-0605-7

Breitburg, D., Grégoire, M., and Isensee, K. (eds): Global Ocean Oxygen Network 2018. The ocean is losing its breath: Declining oxygen in the world's ocean and coastal waters. OC-UNESCO, IOC Technical Series, No. 137, 2018.

Brettar, I., and Rheinheimer, G.: Denitrification in the Central Baltic: evidence for H_2S-oxidation as motor of denitrification at the oxic-anoxic interface. Marine Ecology Progress Series, 77(2-3), 157-169, 1991. http://www.jstor.org/stable/24826569

Bourbonnais, A., Lehmann, M. F., Hamme, R. C., Manning, C. C., and Juniper, S. K.: Nitrate elimination and regeneration as evidenced by dissolved inorganic nitrogen isotopes in Saanich Inlet, a seasonally anoxic fjord. Marine Chemistry, 157, 194–207, 2013. DOI: 10.1016/j.marchem.2013.09.006

Capelle, D. W., Hawley, A. K., Hallam, S. J., and Tortell, P. D.: A multi-year time-series of N_2O dynamics in a seasonally anoxic fjord: Saanich Inlet, British Columbia. Limnology and Oceanography, 63(2), 524-539, 2018. DOI: 10.1002/lno.10645

Carpenter, P. D., Butler, E. C. V., Higgins, H. W., Mackey, D. J., and Nichols, P. D.: Chemistry of trace elements, humic substances and sedimentary organic matter in Macquarie Harbour, Tasmania. Marine and Freshwater Research, 42(6), 625-654, 1991. DOI: 10.1071/MF9910625

Chen, C., Pan, J., Xiao, S., Wang, J., Gong, X., Yin, G., Hou, L., Liu, M., and Zheng, Y.: Microplastics alter nitrous oxide production and pathways through affecting microbiome in estuarine sediments. Water Research 221(118733), 2022. DOI: 10.1016/j.watres.2022.118733

Chen, J., Wells, N. S., Erler, D. V., and Eyre, B. D.: Land-use intensity increases benthic N_2O emissions across three sub-tropical estuaries. Journal of Geophysical Research: Biogeosciences 127, 2022. DOI: 10.1029/2022JG006899

Cresswell, G. R., Edwards, R. J., Barker, B. A.: Macquarie Harbour, Tasmania-seasonal oceanographic surveys in 1985. University of Tasmania Journal contribution. 1989. DOI: 10.26749/rstpp.123.63

de Bie, M. J. M.: Factors controlling nitrification and nitrous oxide production in the Schelde estuary. Doctoral dissertation, Yerseke: Netherlands Institute of Ecology (NIOO-CEMO). 2002.

Dey, R., Lewis, S. C., Arblaster, J. M., and Abram, N. J.: A review of past and projected changes in Australia's rainfall. Wiley Interdisciplinary Reviews: Climate Change, 10(3), e577, 2019. DOI: 10.1002/wcc.577

Etminan, M., Myhre, G., Highwood, E. J., and Shine, K. P.: Radiative forcing of carbon dioxide, methane, and nitrous oxide: A significant revision of the methane radiative forcing. Geophysical Research Letters, 43(24), 12-614, 2016. DOI: 10.1002/2016GL071930

Eyring, V., Gillett, N. P., Achuta Rao, K. M., Barimalala, R., Barreiro Parrillo, M., Bellouin, N., Cassou, C., Durack, P. J., Kosaka, Y., McGregor, S., Min, S., Morgenstern, O., Sun, Y.: Human Influence on the Climate System. In Climate Change 2021: The Physical Science Basis. Contribution of Working Group I to the Sixth Assessment Report of the Intergovernmental Panel on Climate Change. Masson-Delmotte, V., Zhai, P., Pirani, A., Connors, S. L., Péan, C., Berger, S., Caud, N., Chen, Y., Goldfarb, L., Gomis, M. I., Huang, M., Leitzell, K., Lonnoy, E., Matthews, J. B. R., Maycock, T. K., Waterfield, T., Yelekçi, O., Yu, R., and Zhou, B. (eds.): Cambridge University Press, Cambridge, United Kingdom and New York, NY, USA, 423–552, 2021. DOI: 10.1017/9781009157896.005.

Farías, L., Bello, E., Arancibia, G., Fernandez, J.: Distribution of dissolved methane and nitrous oxide in Chilean coastal systems of the Magellanic Sub-Antarctic region (50°– 55°S). Estuarine, Coastal and Shelf Science, 215, 225-240, 2018. DOI: 10.1016/j.ecss.2018.10.020.

Fer, I.: Scaling turbulent dissipation in an Arctic fjord. Deep Sea Research Part II: Topical Studies in Oceanography, 53(1-2), 77-95, 2006. DOI: 10.1016/j.dsr2.2006.01.003

Forster P., Storelvmo T., Armour K., Collins W., Dufresne J.-L., Frame D., Lunt, D., Mauritsen, T., Palmer, M., Watanabe, M., Wild, M.: The earth’s energy budget, climate feedbacks, and climate sensitivity In Climate Change 2021: The Physical Science Basis. Contribution of Working Group I to the Sixth Assessment Report of the Intergovernmental Panel on Climate Change. Masson-Delmotte, V., Zhai, P., Pirani, A., Connors, S. L., Péan, C., Berger, S., Caud, N., Chen, Y., Goldfarb, L., Gomis, M. I., Huang, M., Leitzell, K., Lonnoy, E., Matthews, J. B. R., Maycock, T. K., Waterfield, T., Yelekçi, O., Yu, R., and Zhou, B. (eds.): Cambridge University Press, Cambridge, United Kingdom and New York, NY, USA, 423–552, 2021. DOI: 10.1017/9781009157896.009

Gilbert, D., Rabalais, N. N., Diaz, R. J., & Zhang, J.: Evidence for greater oxygen decline rates in the coastal ocean than in the open ocean. Biogeosciences, 7(7), 2283-2296, 2010. DOI: 10.5194/bg-7-2283-2010

Gillibrand, P. A., Cage, A. G., and Austin, W. E. N.: A preliminary investigation of basin water response to climate forcing in a Scottish fjord: evaluating the influence of the NAO. Continental Shelf Research, 25(5-6), 571-587, 2005. DOI: 10.1016/j.csr.2004.10.011

Grose, M. R., Barnes-Keoghan, I., Corney S. P., White C. J., Holz, G.K., Bennett, J. B., Gaynor, S.M. and Bindof, N.L.: Climate Futures for Tasmania: general climate impacts technical report, Antarctic Climate & Ecosystems Cooperative Research Centre, Hobart, Tasmania, 2010. ISBN: 978-1-921197-05-5

Hartstein, N. D., Maxey, J. D., Loo, J. C. H., and Then, A. Y. H.: Drivers of deep water renewal in Macquarie Harbour, Tasmania. Journal of Marine Systems, 199(103226), 2019. DOI: 10.1016/j.jmarsys.2019.103226

Hashimoto, L. K., Kaplan, W. A., Wofsy, S. C., and McElroy, M. B.: Transformations of fixed nitrogen and N2O in the Cariaco Trench. Deep Sea Research Part A. Oceanographic Research Papers, 30(6), 575-590, 1983. DOI: 10.1016/0198-0149(83)90037-7

Hendzel, L. L., Matthews, C. J. D., Venkiteswaran, J. J., St. Louis, V. L., Burton, D., Joyce, E. M., and Bodaly, R. A.: Nitrous oxide fluxes in three experimental boreal forest reservoirs. Environmental Science & Technology, 39(12), 4353-4360, 2005. DOI: 10.1021/es049443j

Huang, Y., Song, B., Zhang, Q., Park, Y., Wilson, S. J., Tobias, C. R., and An, S.: Seawater intrusion effects on nitrogen cycling in the regulated Nakdong River Estuary, South Korea. Frontiers in Marine Science. 11(1369421), 2024. DOI: 10.3389/fmars.2024.1369421

Inall, M. E., & Gillibrand, P. A.: The physics of mid-latitude fjords: a review. Geological Society, London, Special Publications. 344(1), 17-33, 2010. DOI: 10.1144/SP344.3

Ji, Q., Jameson, B. D., Juniper, S. K., and Grundle, D. S.: Temporal and vertical oxygen gradients modulate nitrous oxide production in a seasonally anoxic fjord: Saanich Inlet, British Columbia. Journal of Geophysical Research: Biogeosciences, 125(9), 2020. DOI: 10.1029/2020JG005631

Kallert, J.: Verteilung von Lachgas (N_2O) und Methan (CH_4) im Fluss Rajang (Malaysia). Bachelor thesis, Christian-Albrecht-University, Kiel, 2017. URI: https://oceanrep.geomar.de/id/eprint/40913/

Kock, A. and Bange, H. W.: Counting the ocean's greenhouse gas emissions, Eos: Earth & Space Science News, 96(3), 10–13, 2015. DOI:10.1029/2015EO023665

Ku, Harry H. "Notes on the use of propagation of error formulas." Journal of Research of the National Bureau of Standards 70, no. 4 (1966). DOI: jresv70Cn4p263_A1b

Kuypers, M. M. M., Marchant, H. K., and Kartal, B.: The microbial nitrogen-cycling network, Nature Reviews Microbiology, 16, 263-276, 2018. DOI: 10.1038/nrmicro.2018.9

Laffoley, D., and Baxter, J. M.: Ocean deoxygenation: Everyone's problem: Causes, impacts, consequences and solutions: Summary for Policy Makers. International Union for Conservation of Nature (IUCN), 2019. DOI: 10.2305/IUCN.CH.2019.13.en

Li, Yuhong, Yang Luo, Jian Liu, Wangwang Ye, Jiexia Zhang, and Liyang Zhan.: Sources and sinks of N_2O in the subtropical Jiulong River Estuary, Southeast China. Frontiers in Marine Science 10 (2023): 1138258. DOI: 10.3389/fmars.2023.1138258

Limburg, Karin E., Denise Breitburg, Dennis P. Swaney, and Gil Jacinto.: Ocean deoxygenation: A primer. One Earth 2, no. 1. 2020: 24-29. DOI: 10.1016/j.oneear.2020.01.001

Lucieer, V.: SeaMap Tasmania Bathymetric Data [data set], Institute for Marine and Antarctic Studies, University of Tasmania, 2007. ISBN: 0-7246-8011-X

Ma, X., Lennartz, S. T., and Bange, H. W. : A multi-year observation of nitrous oxide at the Boknis Eck Time Series Station in the Eckernförde Bay (southwestern Baltic Sea). Biogeosciences, 16(20), 4097-4111, 2019. DOI: 10.5194/bg-16-4097-2019

Macquarie Harbour Dissolved Oxygen Working Group (October 2014), Final Report to the Tasmanian Salmonid Growers Association, 2014.

Maher, D. T., J. Z. Sippo, D. R. Tait, C. Holloway, and Santos, I. R.: Pristine mangrove creek waters are a sink of nitrous oxide. Scientific Reports, 6(25701), 2016. DOI: 10.1038/srep25701

Manning, C. C., Hamme, R. C., & Bourbonnais, A.: Impact of deep-water renewal events on fixed nitrogen loss from seasonally-anoxic Saanich Inlet. Marine Chemistry, 122(1), 1–10, 2010. DOI: 10.1016/j.marchem.2010.08.002

Maxey, J. D., Hartstein, N. D., Penjinus, D., & Kerroux, A.: Simple quality control technique to identify dissolved oxygen diffusion issues with biochemical oxygen demand bottle incubations. Borneo Journal of Marine Science and Aquaculture (BJoMSA), 1, 2017. DOI: 10.51200/bjomsa.v1i.995

Maxey, J. D., Hartstein, N. D., Then, A. Y. H., and Barrenger, M.: Dissolved oxygen consumption in a fjord-like estuary, Macquarie Harbour, Tasmania. Estuarine, Coastal and Shelf Science, 246(107016), 2020. DOI: 10.1016/j.ecss.2020.107016

Maxey, J. D., Hartstein, N. D., Mujahid, A., & Müller, M.: The influence of mesoscale climate drivers on hypoxia in a fjord-like deep coastal inlet and its potential implications regarding climate change: examining a decade of water quality data. Biogeosciences, 19(13), 3131-3150, 2022. DOI: 10.5194/bg-19-3131-2022

McMahon, P. B., and Dennehy, K. F.: N_2O emissions from a nitrogen-enriched river. Environmental Science & Technology, 33(1), 21-25, 1999. DOI: 10.1021/es980645n

Michiels, C. C., Huggins, J. A., Giesbrecht, K. E., Spence, J. S., Simister, R. L., Varela, D. E., Hallam, S. J., Crowe, S. A.: Rates and pathways of N_2 production in a persistently anoxic fjord: Saanich Inlet, British Columbia. Frontiers in Marine Science, 6(27), 2019. DOI: 10.3389/fmars.2019.00027

Mickett, J. B., Gregg, M. C., and Seim, H. E.: Direct measurements of diapycnal mixing in a fjord reach—Puget Sound's Main Basin. Estuarine, Coastal and Shelf Science, 59(4), 539-558, 2004. DOI: 10.1016/j.ecss.2003.10.009

Murray, R. H., Erler, D. V., and Eyre, B. D.: Nitrous oxide fluxes in estuarine environments: response to global change. Global Change Biology, 21(9), 3219-3245, 2015. DOI: 10.1111/gcb.12923

Murray, Rachel, Dirk V. Erler, Judith Rosentreter, Naomi S. Wells, and Bradley D. Eyre.: Seasonal and spatial controls on N_2O concentrations and emissions in low-nitrogen estuaries: Evidence from three tropical systems. Marine Chemistry 221 (2020): 103779. DOI: 10.1016/j.marchem.2020.103779

Musenze, R. S., U. Werner, A. Grinham, J. Udy, and Z. Yuan.: Methane and nitrous oxide emissions from a subtropical estuary (the Brisbane River estuary, Australia). Science of the Total Environment, 472, 719–729, 2014. DOI: 10.1016/j.scitotenv.2013.11.085

Myhre, G., Shindell, D., Bréon, F. M., Collins, W., Fuglestvedt, J., Huang, J., Koch, D., Lamarque, J. F., Lee, D., Mendoza, B., Nakajima, T., Robock, A., Stephens, G., Takemura, T., and Zhang, H.: Anthropogenic and Natural Radiative Forcing. In: Climate Change 2013: The Physical Science Basis. Contribution of Working Group I to the Fifth Assessment Report of the Intergovernmental Panel on Climate Change [Stocker, T.F., Qin, D., Plattner, G. K., Tignor, M., Allen, S. K., Boschung, J, Nauels, A., Xia, Y., Bex, V., and Midgley, P. M.

(eds.)]. Cambridge University Press, Cambridge, United Kingdom and New York, NY, USA, 2013. DOI: 10.1017/CBO9781107415324.018

Myllykangas, J. P., Jilbert, T., Jakobs, G., Rehder, G., Werner, J., and Hietanen, S.: Effects of the 2014 major Baltic inflow on methane and nitrous oxide dynamics in the water column of the central Baltic Sea. Earth System Dynamics, 8(3), 817-826, 2017. DOI: 10.5194/esd-8-817-2017

Nevison, C., and Holland, E.: A reexamination of the impact of anthropogenically fixed nitrogen on atmospheric N_2O and the stratospheric O_3 layer. Journal of Geophysical Research: Atmospheres, 102(D21), 25519-25536, 1997. DOI: 10.1029/97JD02391

Orif, M. I., Yasar N. K., Radwan K. A., and Sudheesh, V.: Deoxygenation turns the coastal Red Sea lagoons into sources of nitrous oxide. Marine Pollution Bulletin 189(114806), 2023. DOI: 10.1016/j.marpolbul.2023.114806

Portmann, R. W., Daniel, J. S., and Ravishankara, A. R.: Stratospheric ozone depletion due to nitrous oxide: influences of other gases. Philosophical Transactions of the Royal Society B, 367, 1256–1264, 2012. DOI: 10.1098/rstb.2011.0377

Raes, E. J., Bodrossy, L., Van de Kamp, J., Holmes, B., Hardman-Mountford, N., Thompson, P. A., McInnes, A. S., Waite, A. M.: Reduction of the powerful greenhouse gas N_2O in the South-Eastern Indian Ocean. PLoS One, 11(1), 2016. DOI: 10.1371/journal.pone.0145996

Ravishankara, A. R., Daniel, J. S., and Portmann, R. W.: Nitrous oxide (N_2O): the dominant ozone-depleting substance emitted in the 21st century. Science, 326(5949), 123-125, 2009. DOI: 10.1126/science.1176985

Raymond, P. A., and Cole, J. J.: Gas exchange in rivers and estuaries: Choosing a gas transfer velocity. Estuaries, 24(2), 312-317, 2001. DOI: 10.2307/1352954

Reading, M. J., Santos, I. R., Maher, D. T., Jeffrey, L. C., and Tait, D. R.: 2017. Shifting nitrous oxide source/sink behaviour in a subtropical estuary revealed by automated time series observations. Estuarine, Coastal and Shelf Science, 194: 66-76, 2017. DOI: 10.1016/j.ecss.2017.05.017

Reading, M. J., Tait, D. R., Maher, D. T., Jeffrey, L. C., Looman, A., Holloway, C., Shishaye, H. A., Barron, S. and Santos, I. R.: Land use drives nitrous oxide dynamics in estuaries on regional and global scales. Limnology and Oceanography, 65(8), 1903-1920, 2020. DOI: 10.1002/lno.11426

Reading, M.J.: Aquatic nitrous oxide dynamics from rivers to reefs. Doctoral dissertation, Southern Cross University, 2022. DOI: 10.25918/thesis.197

Resplandy, Laure, Allison Hogikyan, Jens Daniel Müller, R. G. Najjar, Hermann W. Bange, Daniele Bianchi, T. Weber, W.-J. Cai, S. C. Doney, K. Fennel, M. Gehlen, J. Hauck, F. Lacroix, P. Landschützer, C. Le Quéré, A. Roobaert, J. Schwinger, S. Berthet, L. Bopp, T. T. T. Chau, M. Dai, N. Gruber, T. Ilyina, A. Kock, M. Manizza, Z. Lachkar, G. G. Laruelle, E. Liao, I. D. Lima, C. Nissen, C. Rödenbeck, R. Séférian, K. Toyama, H. Tsujino, P. Regnier.: A synthesis of global coastal ocean greenhouse gas fluxes. Global biogeochemical cycles 38, no. 1 2024: e2023GB007803. DOI: 10.1029/2023GB007803

Rönner, U.: Distribution, production and consumption of nitrous oxide in the Baltic Sea. Geochimica et Cosmochimica Acta, 47(12), 2179-2188, 1983. DOI: 10.1016/0016-7037(83)90041-8

Rosentreter, J. A., Wells, N. S., Ulseth, A. J., and Eyre, B. D.: Divergent gas transfer velocities of CO_2, CH_4, and N_2O over spatial and temporal gradients in a subtropical estuary. Journal of Geophysical Research: Biogeosciences, 126(10), 2021. DOI: 10.1029/2021JG006270

Rosentreter, J.A., Laruelle, G.G., Bange, H.W., Bianchi, T.S., Busecke, J.J., Cai, W.J., Eyre, B.D., Forbrich, I., Kwon, E.Y., Maavara, T. and Moosdorf, N.: Coastal vegetation and estuaries are collectively a greenhouse gas sink. Nature Climate Change, 13(6), 579-587, 2023. DOI: 10.1038/s41558-023-01682-9

Sánchez-Rodríguez, J., Sierra, A., Jiménez-López, D., Ortega, T., Gómez-Parra, A., and Forja, J.: Dynamic of CO_2, CH_4 and N_2O in the Guadalquivir estuary. Science of The Total Environment, 805, 2022. DOI: 10.1016/j.scitotenv.2021.150193

Schulz, G., Sanders, T., Voynova, Y. G., Bange, H. W., and Dähnke, K.: Seasonal variability of nitrous oxide concentrations and emissions in a temperate estuary. Biogeosciences, 20(15), 3229-3247, 2023. DOI: 10.5194/bg-20-3229-2023

Schweiger, B.: Messung von NH_2OH in ausgewaehlten Seegebieten. Master thesis, Leibniz Institute of Marine Science, Kiel (IFM-GEOMAR), 2006.

Seitzinger, S. P., Kroeze, C., and Styles, R. V.: Global distribution of N_2O emissions from aquatic systems: natural emissions and anthropogenic effects. Chemosphere-Global Change Science, 2(3-4), 267-279, 2000. DOI: 10.1016/S1465-9972(00)00015-5

Sierra, A., Jiménez-López, D., Ortega, T., Gómez-Parra, A., and Forja, J.: Factors controlling the variability and emissions of greenhouse gases (CO_2, CH_4 and N_2O) in three estuaries of the Southern Iberian Atlantic Basin during July 2017. Marine Chemistry, 226(103867), 2020. DOI: 10.1016/j.marchem.2020.103867

Salamena, G. G., Whinney, J. C., Heron, S. F., and Ridd, P. V.: Internal tidal waves and deep-water renewal in a tropical fjord: Lessons from Ambon Bay, eastern Indonesia. Estuarine, Coastal and Shelf Science, 253(107291), 2021. DOI: 10.1016/j.ecss.2021.107291

Salamena, G. G., Whinney, J. C., Heron, S. F., and Ridd, P. V.: Frontogenesis and estuarine circulation at the shallow sill of a tropical fjord: Insights from Ambon Bay, eastern Indonesia. Regional Studies in Marine Science, 56(102696), 2022. DOI: 10.1016/j.rsma.2022.102696

Smith, R. W., Bianchi, T. S., Allison, M., Savage, C., and Galy, V.: High rates of organic carbon burial in fjord sediments globally, Nature Geoscience, 8(6), 450-453, 2015. DOI: 10.1038/ngeo2421

Stow, C. A., Walker, J. T., Cardoch, L., Spence, P., and Geron, C.: N_2O emissions from streams in the Neuse River watershed, North Carolina. Environmental Science & Technology, 39(18), 6999-7004, 2005. DOI: 10.1021/es0500355

Sturm, K., Werner, U., Grinham, A., and Yuan, Z.: Tidal variability in methane and nitrous oxide emissions along a subtropical estuarine gradient. Estuarine, Coastal and Shelf Science, 192, 159–169, 2017. DOI: 10.1016/j.ecss.2017.04.027

Suntharalingam, P., and Sarmiento, J. L.: Factors governing the oceanic nitrous oxide distribution: Simulations with an ocean general circulation model. Global Biogeochemical Cycles, 14(1), 429-454, 2000. DOI: 10.1029/1999GB900032

Tait, D. R., Maher, D. T., Wong, W., Santos, I. R., Sadat-Noori, M., Holloway, C., and Cook, P. L. M.: Greenhouse gas dynamics in a salt-wedge estuary revealed by high resolution cavity ringdown spectroscopy observations. Environmental Science & Technology, 51: 13771–13778, 2017. DOI: 10.1021/acs.est.7b04627

Tang, Weiyi, Jeff Talbott, Timothy Jones, and Bess B. Ward: Variable contribution of wastewater treatment plant effluents to downstream nitrous oxide concentrations and emissions. Biogeosciences 21, no. 14, 3239-3250, 2024. DOI: 10.5194/bg-21-3239-2024

Teasdale, P. R., Apte, S. C., Ford, P. W., Batley, G. E., and Koehnken, L.: Geochemical cycling and speciation of copper in waters and sediments of Macquarie Harbour, Western Tasmania. Estuarine, Coastal and Shelf Science, 57(3), 475-487, 2003. DOI: 10.1016/S0272-7714(02)00381-5

Testa, Jeremy M., Jacob Carstensen, Arnaud Laurent, and Ming Li.: Hypoxia and Climate Change in Estuaries. In Climate Change and Estuaries, pp. 143-170. CRC Press, 2023. ISBN: 9781003126096

Walinsky, S. E., Prahl, F. G., Mix, A. C., Finney, B. P., Jaeger, J. M., and Rosen, G. P.: Distribution and composition of organic matter in surface sediments of coastal Southeast Alaska, Continental Shelf Research, 29(13), 1565-1579, 2009. DOI: 10.1016/j.csr.2009.04.006

Walter, S., Bange, H. W., and Wallace, D. W.: Nitrous oxide in the surface layer of the tropical North Atlantic Ocean along a west to east transect. Geophysical Research Letters, 31(23), 2004. DOI: 10.1029/2004GL019937

Walter, S., Breitenbach, U., Bange, H. W., Naucsh, G., and Wallace, D. W. R.: Distribution of N_2O in the Baltic Sea during transition from anoxic to oxic conditions. Biogeosciences, 3, 557-570, 2006. DOI: 10.5194/bg-3-557-2006

Wan, X. S., Lin, H., Ward, B. B., Kao, S., and Dai M.: Significant seasonal N_2O dynamics revealed by multi-year observations in the Northern South China Sea. Global Biogeochemical Cycles, 36(10), 2022. DOI: 10.1029/2022GB007333

Weiss, R. F. and Price, B. A.: Nitrous oxide solubility in water and seawater, Marine Chemistry, 8, 347-359, 1980. DOI: 10.1016/0304-4203(80)90024-9

Wells, N. S., Maher, D. T., Erler, D. V., Hipsey, M., Rosentreter, J. A., and Eyre, B. D.: Estuaries as sources and sinks of N_2O across a land use gradient in subtropical Australia. Global Biogeochemical Cycles, 32, 877–894, 2918. DOI: 10. 1029/2017GB005826

Willis, M.: Tascatch Variation 2 – Surface Water Models (Document ID Number WR 2008/005). Department of Primary Industries and Water. Hydro Tasmania Consulting, https://nre.tas.gov.au /water/water-monitoring-and-assessment/hydrological assessment/tasmanian-catchmentsmodelling /surface-water-models. 2008.

Wilson, S. T., Bange, H. W., Arévalo-Martínez, D. L., Barnes, J., Borges, A. V., Brown, I., Bullister, J. L., Burgos, M., Capelle, D. W., Casso, M., de la Paz, M., Farías, L., Fenwick, L., Ferrón, S., Garcia, G., Glockzin, M., Karl, D. M., Kock, A., Laperriere, S., Law, C. S., Manning, C. C., Marriner, A., Myllykangas, J. P., Pohlman, J. W., Rees, A. P., Santoro, A. E., Tortell, P. D., Upstill-Goddard, R. C., Wisegarver, D. P., Zhang, G. L., and Rehder, G.: An intercomparison of oceanic methane and nitrous oxide measurements, Biogeosciences, 15, 5891-5907, 2018. DOI: 10.5194/bg-15-5891-2018

Wilson, S. T., Al-Haj, A. N., Bourbonnais, A., Frey, C., Fulweiler, R. W., Kessler, J. D., Marchant, H. K., Milucka, J., Ray, N. E., Suntharalingham, P., Thornton, B. F., Upstill-Goddard, R. C., Weber, T. S., Arévalo-Martínez, D. L., Bange, H. W., Benway, H. M., Bianchi, D., Borges, A. V., Chang, B. X., Crill, P. M., del Valle, D. A., Farías, L., Joye, S. B., Kock, A., Labidi, J., Manning, C. C., Pohlman, J. W., Rehder, G., Sparrow, K. J., Tortell, P. D., Treude, T., Valentine, D. L., Ward B. B., Yang, S., and Yurganov, L. N.: Ideas and perspectives: A strategic assessment of methane and nitrous oxide measurements in the marine environment. Biogeosciences, 17, 5809-5828, 2020. DOI: 10.5194/bg-17-5809-2020

Wu, L., Chen X., Wei, W., Liu, Y., Wang, D., and Ni, B.: A critical review on nitrous oxide production by ammonia-oxidizing archaea. Environmental Science & Technology 54(15), 9175-9190, 2020. DOI: 10.1021/acs.est.0c03948

Yevenes, M. A., Bello, E., Sanhueza-Guevara, S., and Farías, L.: Spatial distribution of nitrous oxide (N_2O) in the Reloncaví estuary–sound and adjacent sea (41–43 S), Chilean Patagonia. Estuaries and Coasts, 40, 807-821, 2017. DOI: 10.1007/s12237-016-0184-z

Yoshinari, T.: Nitrous oxide in the sea. Marine Chemistry 2(4), 189–202, 1976. DOI: 10.1016/0304-4203(76)90007-4.

Zappa, C. J., Raymond, P. A., Terray, E. A., and McGillis, W. R.: Variation in surface turbulence and the gas transfer velocity over a tidal cycle in a macro-tidal estuary. Estuaries, 26, 1401-1415, 2003. DOI: 10.1007/BF02803649

Zhang, G. L., Zhang, J., Liu, S. M., Ren, J. L., and Zhao. Y. C.: Nitrous oxide in the Changjiang (Yangtze River) Estuary and its adjacent marine area: Riverine input, sediment release and atmospheric fluxes. Biogeosciences 7(11), 3505-3516, 2010. DOI: 10.5194/bg-7-3505-2010